A Review of DC Fast Chargers with BESS for Electric Vehicles: Topology, Battery, Reliability Oriented Control and Cooling Perspectives

Polat, Hakan; Hosseinabadi, Farzad; Hasan, Md Mahamudul; Chakraborty, Sajib; Geury, Thomas; El Baghdadi, Mohamed; Wilkins , Steven; Hegazy, Omar

Published in:
Open access journal Batteries- Special Issue on Advances in Charging Systems and Charging Management Strategies for Battery Electric Vehicles

DOI:
10.3390/batteries9020121

Publication date:
2023

batteries

MDPI

Review

A Review of DC Fast Chargers with BESS for Electric Vehicles: Topology, Battery, Reliability Oriented Control and Cooling Perspectives

Hakan Polat [1,2], Farzad Hosseinabadi [1,2], Md. Mahamudul Hasan [1,2], Sajib Chakraborty [1,2], Thomas Geury [1,2], Mohamed El Baghdadi [1,2], Steven Wilkins [3] and Omar Hegazy [1,2,*]

1 MOBI-EPOWERS Research Group, ETEC Department, Vrije Universiteit Brussel, Pleinlaan 2, 1050 Brussels, Belgium
2 Flanders Make, Gaston Geenslaan 8, 3001 Heverlee, Belgium
3 TNO, 5700 AT Helmond, The Netherlands
* Correspondence: omar.hegazy@vub.be

Abstract: The global promotion of electric vehicles (EVs) through various incentives has led to a significant increase in their sales. However, the prolonged charging duration remains a significant hindrance to the widespread adoption of these vehicles and the broader electrification of transportation. While DC-fast chargers have the potential to significantly reduce charging time, they also result in high power demands on the grid, which can lead to power quality issues and congestion. One solution to this problem is the integration of a battery energy storage system (BESS) to decrease peak power demand on the grid. This paper presents a review of the state-of-the-art use of DC-fast chargers coupled with a BESS. The focus of the paper is on industrial charger architectures and topologies. Additionally, this paper presents various reliability-oriented design methods, prognostic health monitoring techniques, and low-level/system-level control methods. Special emphasis is placed on strategies that can increase the lifetime of these systems. Finally, the paper concludes by discussing various cooling methods for power electronics and stationary/EV batteries.

Keywords: EV DC-fast charging; battery energy storage system (BESS); EV charger topology; reliability; battery; reliability oriented control; BESS cooling; EV battery cooling

Citation: Polat, H.; Hosseinabadi, F.; Hasan, M.M.; Chakraborty, S.; Geury, T.; El Baghdadi, M.; Wilkins, S.; Hegazy, O. A Review of DC Fast Chargers with BESS for Electric Vehicles: Topology, Battery, Reliability Oriented Control and Cooling Perspectives. *Batteries* **2023**, *9*, 121. https://doi.org/10.3390/batteries9020121

Academic Editor: Federico Baronti

Received: 2 January 2023
Revised: 29 January 2023
Accepted: 6 February 2023
Published: 8 February 2023

1. Introduction

The use of electric vehicles (EVs) is being incentivized globally as a replacement for traditional internal combustion engine vehicles (ICEVs) [1]. This shift towards EVs is driven by the limited availability of fossil fuels and the increasing investment in renewable energy sources such as solar and wind power. The scarcity of fossil fuels has led countries to invest in these alternative forms of energy, and the same is now happening with EVs [2]. Approximately 17% of all greenhouse gas emissions globally are a result of transportation [3]. This transition from ICEVs to EVs is therefore driven not only by economic considerations but also by concerns for the environment. However, it should be noted that EVs have a shorter range than ICEVs, which can lead to "range anxiety" among consumers [4]. The limitation in the range of EVs is primarily due to the weight of the batteries. In contrast to ICEVs, where a larger gasoline tank results in a higher range, increasing the size and weight of the battery in EVs does not necessarily lead to a significantly longer range [5]. Therefore, the need for more frequent charging of EVs compared to ICEVs is a concern that needs to be addressed in the near future. Additionally, even if it were possible to replace or supplement all gasoline stations with EV charging stations, the waiting times for charging, which can range from 15–20 min to several hours, depending on the technology and power level of the charger, is a potential issue that will have to be addressed [6]. The long waiting time and the need for more frequent charging of EVs indicate that EV charging

infrastructure must be distributed throughout cities and towns, or along highways, rather than concentrated in a few large charging stations, to avoid long lines and wait times. This approach would provide more convenient and accessible charging options for EV owners, and help to overcome one of the main barriers to the widespread adoption of EVs.

The integration of renewable energy sources into the conventional power grid presents a challenge due to the lack of storage units. This makes it difficult to maintain a balance between supply and demand. As the proportion of renewable energy in the grid increases, the total grid inertia decreases, leading to higher frequency oscillations during sudden changes in demand or surplus conditions. This highlights the need for effective energy storage solutions to ensure a stable and reliable power grid [7].

The commonly recognized phenomenon known as the "duck curve" is illustrated in Figure 1. This curve represents the fluctuation of demand for electricity on the grid in the state of California, as reported in reference [8]. While the curve may vary slightly on a daily basis, on average, it is observed that there is a significant increase in demand between the hours of 5 p.m. and 9 p.m. As incentives for electrification continue to be implemented in various sectors, including transportation, household appliances, and industrial machinery, the use of electrical equipment in daily life is increasing. As a result, when individuals return home from work in the evening, there is a sudden surge in demand for electricity. However, if the rate of change of power demand is substantial, it can cause instability in the grid as conventional coal and gas power plants are unable to adjust their output as rapidly as required to meet the fluctuation in demand.

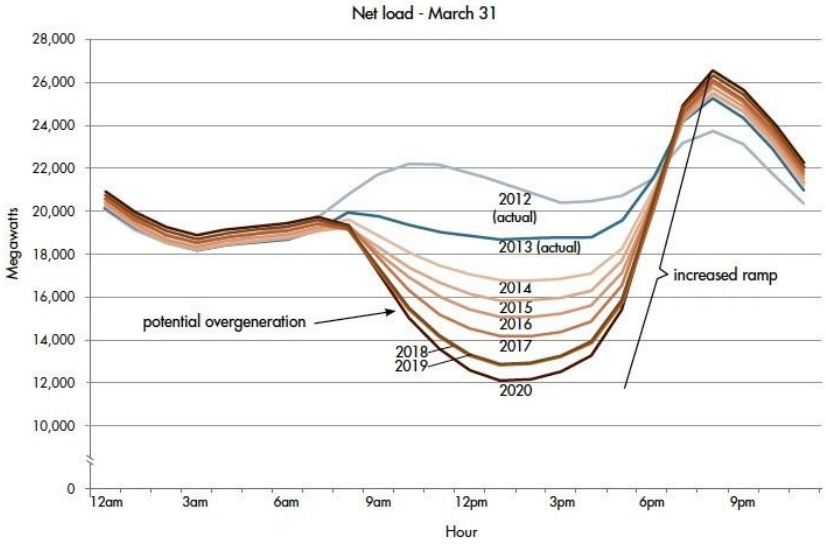

Figure 1. A common duck curve in California, USA [8].

Furthermore, as the sun sets, the absence of storage in photovoltaic (PV) generation leads to an increased reliance on fossil fuels. Additionally, while wind power is a renewable resource, its unpredictability poses a challenge. It is anticipated that individuals will likely charge their EVs at home or at fast charging stations prior to or following work. However, home-installed EV chargers are often slow AC overnight chargers that require a significant amount of time to charge [9]. To mitigate this issue, researchers have proposed various smart charging methods to reduce power demand on the grid side, as discussed in the literature by Kriukov et al. [10] and Hua et al. [11]. Additionally, there has been a growing focus on utilizing EVs as mobile energy storage systems for vehicle-to-grid (V2G) operations and storing excess solar power in EV batteries. While these smart charging methods may help to flatten the demand curve, local energy storage systems are considered to be the primary solution for reducing sharp changes in power demand.

A representation of the DC-Fast charger with BESS is presented in Figure 2. The idea behind using DC-fast charging with a battery energy storage system (BESS) is to supply

the EV from both grid and the battery at the same time [12]. This way the demand from the grid is smaller. Once the charging is complete and the EV is disconnected, however, the battery is charged even in the absence of an EV. Therefore, the same amount of energy is absorbed from the grid over a longer period of time [13]. Another practical reason is the grid's capability to supply the demanded power. In rural areas and highways, a weak grid may not be able to provide the demanded power. Considering that one of the main problems slowing down the transition from ICEV to EV is "range anxiety", highways are especially where fast charging needs to be present. Therefore, having BESS may reduce the grid infrastructure cost.

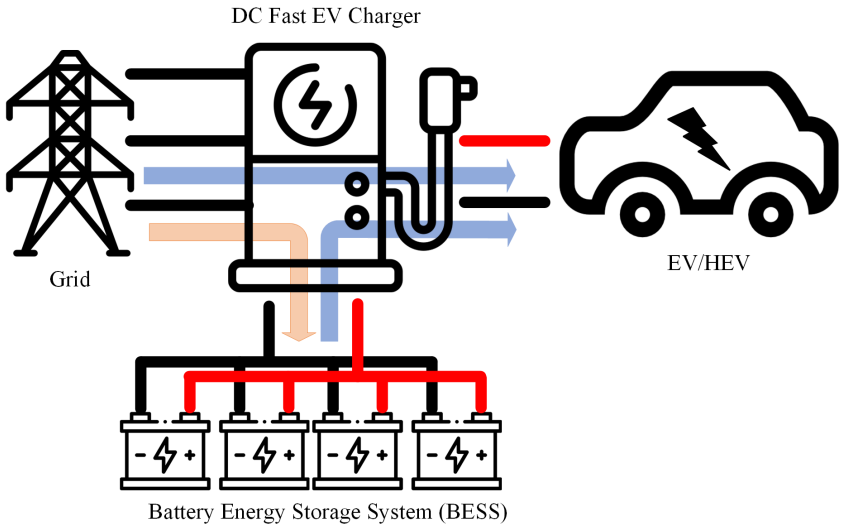

Figure 2. A representation of grid-connected DC-Fast charger with local BESS. Light blue arrows show the direction of the active power flow when EV is connected. Light orange arrow shows the direction of active power flow when EV charging is finished.

With the incentives towards EVs, R&D on different battery technologies has significantly increased. Mass production of batteries, especially Li-ion, significantly decreased the cost, and stationary BESS is becoming more feasible. Considering [14,15], utility-scale BESS will be more profitable in the upcoming years even from the point of a conservative estimation approach. However, depending on the grid strength and system sizing, batteries may be subject to high C-rates, high number of cycling, and deep discharging which directly affects the overall lifetime of the battery unit [16]. Similarly, for power electronics, semiconductor selection, cooling strategy, and capacitor selection are key for proper design with high reliability [17]. Considering that DC-fast chargers are required mostly during long journeys in rural areas, maintenance has to be minimized and predictive to reduce operational costs. Battery diagnostics, and online power electronics predictive health monitoring [18] are required in order to take action to further improve the lifetime of the overall system.

In [13], a comprehensive review for DC-Fast chargers with BESS is made where the focus is topologies, technologies (fuel-cell, battery, flywheel), and comparison of these technologies in terms of system sizing, efficiency, and volume. In [19], a comprehensive review of topology and control methods for EV fast charging is made. In [9], additional focus is given to state-of-the-art standards for EV charging including inductive power transfer. In [20], EV charging is investigated only for extreme fast charging stations including direct medium voltage connected chargers. These papers have a broad spectrum in EV charging, a comprehensive review for DC-fast chargers with BESS focusing on reliability-oriented control, cooling, and battery technology is missing. This paper aims to include an in-depth comparison of different topologies and battery chemistries, from the point of view of industrial application. In the second section, the architecture and the different topologies

are presented. Later, the battery technologies including second-life batteries are discussed and compared from operational cost, cyclability, and reliability. In the fourth section, topics such as failure mechanism and design for reliability are key for an improved lifetime of the overall charger focusing on prognostics and health management (PHM). Later, both low and system-level control methods for different topologies including control for reliability are presented. The paper is finally concluded with thermal management and smart battery pre-conditioning strategies for both power electronics and stationary BESS.

2. Architectures and Topologies

With the recent progress in EV technology, the charging industry has also developed flexible charging units. In Table 1, some of the most popular commercial DC fast chargers are presented. As can be seen in Table 1, the power levels are different to address a wider segment of customers. As an example, ABB Terra HP is a modular charger capable of supplying multiple vehicles with variable power. Similarly, EVBox and Heliox provide their customers with the option to choose the power level. Another important feature of these chargers is the output voltage range. Most of the state-of-the-art chargers are capable of supplying the 200–1000 V range. A limit for DC fast charging is the current limit imposed by the vehicle. Indeed, while the EV charger is capable of supplying high power, that does not necessarily imply that the EV can be charged with high power. As an example even if a Nissan Leaf is connected to a 150 kW charger, the power will be still limited to 46 kW, therefore resulting in a longer charging time [21]. Hence, it is expected that the automotive industry will shift towards battery pack configurations with higher voltage ratings [22]. The charging industry has already prepared for such a transition. Moreover, the majority of EV trucks and buses are designed with 800 V batteries [23]. So, the EV chargers presented in Table 1 are capable of charging both 400 V and 800 V batteries which makes them flexible and multi-use.

Table 1. State-of-the-art DC fast charging solutions in the industry (NP: not provided).

Manufacturer	ABB Terra HP [24]	ABB Terra 54 [25]	Siemens VersiCharge Ultra 175 [26]	EVBox Troniq Modular [27]	Tesla SuperCharger [28]	Heliox Rapid 50–300 kW [29]
Power	up to 350 kW	50 kW	175 kW	up to 240 kW	135 kW	up to 300 kW
Input Voltage	400 VAC	480 VAC	380–480 VAC	400 VAC	380–480 VAC	400 VAC
Output Voltage	150–920 VDC	200–500 VDC	200–920 VDC	150–920 VDC	40–410 V	150–500 VDC
Multiport	Yes	Yes	Yes	Yes	Yes	Yes
Efficiency	95%	94%	96%	95%	91%	>94%
Time to add 100 km	<3 min @350 kW	N.P.	<6 min @175 kW	<4.5 min @240 kW	<11 min @135 kW	<4 min @300 kW

A conventional charging system consists of a grid, an AC/DC stage, and a DC/DC stage. The system architecture of a DC-Fast charger station with BESS is presented in Figure 3. For each stage, different conversion types are denoted from 1 to 10. It is important to note that not all configurations are possible due to the requirement for isolation of the batteries, renewables, and the grid [30,31]. As an example for the variable DC-Bus case, 1 can be combined with 5-6-7; while for 4, it is not possible to connect with 5 and 6 due to a lack of isolation between the grid and the EV/stationary batteries. The different parts of the system and possible topologies are explained in detail in the following sections.

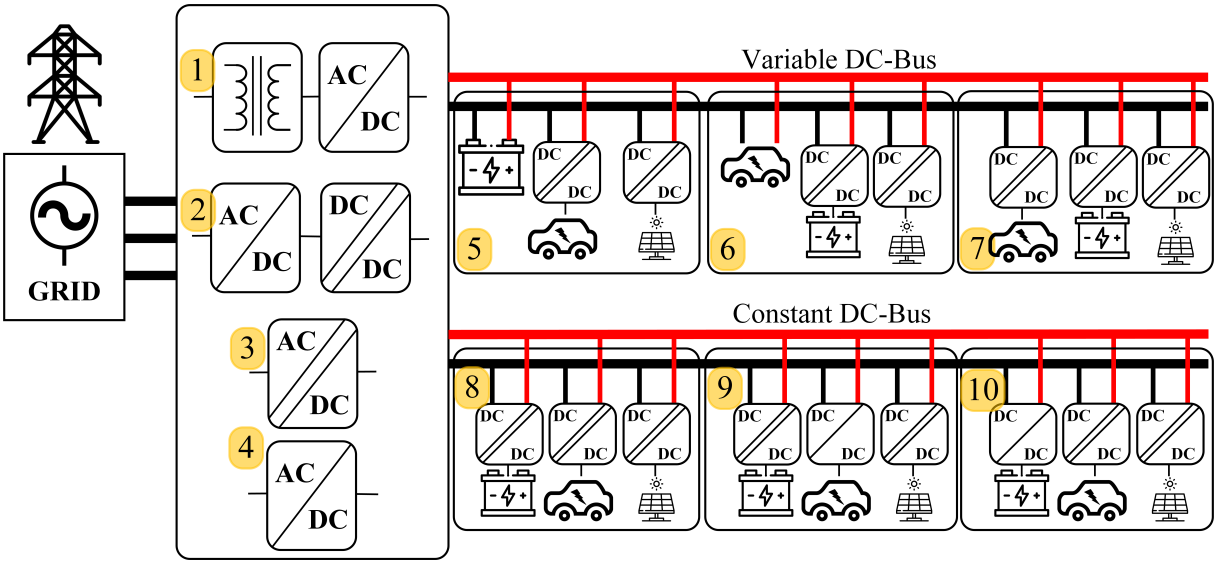

Figure 3. Architecture of a DC-Fast charger with BESS for different cases. Not all cases are compatible with each other.

2.1. Variable DC-Bus

Regardless of the application of the battery module(stationary or EV), the battery voltage is related to its state of charge (SoC). Therefore, battery chargers require a variable output voltage. The idea behind a variable DC-bus is to connect the battery or EV battery directly to the DC-bus, where the DC-bus voltage is always equal to the battery voltage (cannot be both due to isolation requirements). Therefore, a DC/DC stage can be omitted in the design, resulting in a system with lower cost and higher efficiency. However, such an architecture has lower scalability compared to a constant DC-Bus since no other EV can be directly connected to the DC-Bus. Moreover, it does not allow the direct connection of multiple batteries with different chemistries.

Another downside of variable DC-Bus is the fact that isolated DC/DC converters require a wider input and output voltage range which complicates the design procedure. As an example, a common topology used in isolated DC/DC is the dual active bridge (DAB) converter [32]. In order to increase the efficiency the leakage inductor has to be designed as small as possible. However, a small leakage inductor results in a narrow zero voltage switching (ZVS) range for a specific voltage transfer ratio and power transfer [33]. Therefore, compared to constant DC-Bus the efficiencies of the isolated DC/DC stages may be lower.

2.2. Constant DC-Bus

Unlike variable DC-Bus, having constant voltage results in the requirement of a DC/DC converter for each component. If the isolation is satisfied with the grid side, either EV or the BESS DC/DC stage can be non-isolated which will result in increased system efficiency. However, the system will be then non-scalable. Compared to variable DC-Bus, the input voltage range of the DC/DC converters is narrower. Therefore, the efficiencies of these converters will be higher. However, if the grid connection is weak (low short-circuit MVA), the DC/DC converter connecting BESS with the DC-Bus must have a high power rating. It can even be comparable to the DC/DC for the EV.

2.3. AC/DC Conversion Stage Topologies

Independent of which type of DC-Bus strategy is used the first stage converts the 3-phase AC from the grid to DC. Cases 1, 2, and 4 consist of a non-isolated AC/DC stage whereas case 3 consists of an AC/DC stage with a high-frequency isolation transformer. Some of the most common AC/DC topologies are presented in Figure 4.

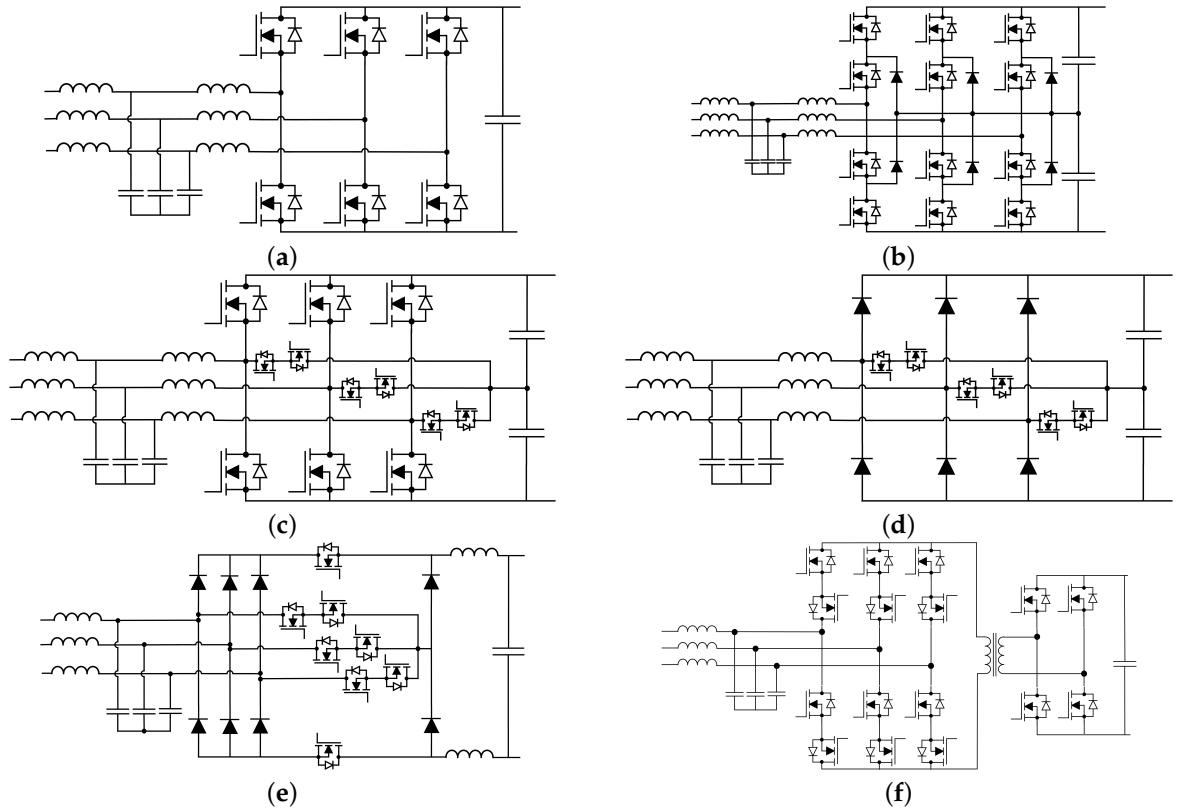

Figure 4. Different AC/DC conversion topologies connected to a three-phase AC grid. Grid drawings are omitted for visual clarity: (**a**) Two-level active front end (AFE); (**b**) Three-level neutral point clamped (NPC) AFE; (**c**) Three-level T-type AFE; (**d**) Vienna rectifier; (**e**) Swiss rectifier; (**f**) Matrix Converter-based isolated AC/DC converter [34].

The most conventional topology is the 2-level AFE presented in Figure 4a [35]. It consists of only six switches. Depending on the technology of the switches, it is possible to transfer power in both directions. In order to comply with grid standards it is often connected to the grid with an LCL filter (possibly higher order filters). If isolation is required, the grid side inductor is replaced with a low-frequency transformer [36]. In Figure 4b,c 3-lvl NPC-AFE [37] and T-type AFE [38] are presented, respectively. These topologies are superior to 2-level AFE in terms of smaller filter [39], improved THD, lower semiconductor stress, reduced total inverter loss, and improved cooling due to improved loss distribution with an increased number of switches. The 3-level NPC-AFE consists of 12 switches and 6 diodes whereas T-type AFE has only 12 switches. Both topologies have a 5-level voltage waveform that reduces the need for filtering hence they both have reduced filter size [40]. The major difference between the two is the semiconductor voltage stresses. While the 3-level NPC-AFE has the semiconductor voltage stress of $\frac{V_{DC}}{2}$ on all switches; in T-type topology, the line switches are subject to V_{DC} and the common source connected switches (neutral switches) are subject to $\frac{V_{DC}}{2}$. Both topologies require DC-link capacitor voltage balancing [41].

In Figure 4d, the Vienna rectifier is presented [42]. Compared to 3-level T-type and NPC-AFE, the Vienna rectifier uses six diodes and six switches. It is hence cheaper and requires fewer active-controlled switches. It has all the advantages of a 3-level. However, a downside of this topology is the fact that it is uni-directional and the need for active control for DC-link voltage balancing. Moreover, for a 400 V_{l-l} grid, 1200 V diodes are required whereas the switch voltage stress is $\frac{V_{DC}}{2}$. Compared to other topologies in Figure 4, Swiss rectifiers are buck-type AC/DC converters [43]. They consist of eight diodes and eight active switches. A fast charger is most commonly connected to a 400 V 3-phase grid and a small passenger EV with a 400 V battery is often charged using a fast charger.

Therefore, the Swiss rectifier is suitable for low-voltage EV charging. If a wide output range is required it is recommended to use a series-connected DC/DC stage. Compared to other topologies, the switches are subject to less voltage stress; therefore, 400 V grid-connected Swiss rectifiers can use 900 V rated switches and diodes [44]. Finally, in Figure 4e, a matrix converter-based single-stage isolated AC/DC converter is presented. It consists of 16 active switches and a high-frequency transformer. Compared to other topologies it does not require a low-frequency grid-connected transformer or a series-connected isolated DC/DC stage. However, a downside of this topology is the number of active controlled switches and the requirement for complex control. The efficiency of matrix converters is significantly affected by the control methodology. In Table 2, the investigated AC/DC topologies are listed and compared according to their merits (best colored in green, worst colored in red.).

Table 2. Comparison of AC/DC Topologies. The excelling topology for the specific feature is colored green: best, red: worst.

Topology	Type	#of Switch	Power Direction	Isolation	Semiconductor Voltage Stress	Filter Size	Power Density	Control
2-Level AFE	Boost	6 Active + 0 Passive	Bi-directional	No	Vdc	Large	Low	Simple
3-Level NPC AFE	Boost	12 Active + 6 Passive	Bi-directional	No	Vdc/2	Small	High	Moderate
T-Type AFE	Boost	12 Active + 0 Passive	Bi-directional	No	Vdc, Vdc/2	Small	High	Moderate
Vienna Rectifier	Boost	6 Active + 6 Passive	Uni-directional	No	Vdc, Vdc/2	Small	High	Moderate
Swiss Rectifier	Buck	8 Active + 8 Passive	Uni-directional	No	Vdc,Vdc/2	Smallest	High	Complex
Matrix Converter	Variable	16 Active + 0 Passive	Bi-directional	Yes	Variable	Variable	Highest	Complex

2.4. DC/DC Topologies

Regardless of any architecture, both the batteries and the EVs are often connected to a common DC-bus using a DC/DC converter. Clearly, the DC/DC stage connected to the BESS has to be bi-directional. However, there is no such need for the EV stage. In the literature, the feasibility of using EV batteries as local storage units is often investigated [45,46]. The aim is to store the extra energy generated by the renewables in the EV battery and absorb it back to the grid when there is increased power demand, and hence flatten the duck curve presented in Figure 1.

Considering that DC-fast chargers are used in rural areas, highways, and fast charging stations, it is unlikely for any vehicle to stay overnight and provide grid service. Because the aim of increasing the charger power is to decrease the charging time. However, as also stated in this paper before in Table 1, the companies are trying modular structures capable of charging both passenger EVs and public buses or trucks. In many cities, a lower amount of buses are working after certain hours. Considering an average electric public bus has 150 kWh of battery installed, they have great potential for BESS providing grid service [47]. In conclusion, if only a small passenger EV will be charged it is unnecessary to use bi-directional DC/DC converters on the EV to DC-bus connection. However, if grid service is expected from the system, it may also be bi-directional provided that the AC/DC stage is also bi-directional.

In Figure 3, if the isolation is satisfied in the AC/DC stage, non-isolated DC/DC converters can be used as shown in cases 9 and 10. It is common knowledge that non-isolated DC/DC converters have higher efficiency and power density compared to isolated DC/DC converters due to the lack of high-frequency transformers which as a rule of thumb often contributes as much as total semiconductor loss [44,48]. Therefore, in this section, DC/DC converters will be investigated in two parts.

2.4.1. Isolated DC/DC Converters

In Figure 5, common isolated DC/DC topologies employed in EV/battery charging are presented.

With the recent development in semiconductor technology such as GaN and SiC, the conduction and switching losses decreased significantly [49]. Moreover, with the improvement in micro-controller capabilities and new magnetic material, dual active bridge

(DAB) became an industry favorite due to its simplicity, a low number of components, high efficiency, and high power density [50]. It consists of four bi-directional switches on both the primary and secondary sides. The coupling is achieved using a high-frequency transformer. DAB power is controlled by controlling the phase shift between the primary and secondary side voltages [51]. The phase shift control of the power is bi-directional and assuming the fundamental harmonic of voltage waveforms the equation is the same as the active power flow equation. DAB converter can also achieve ZVS that results in a high efficiency without any resonant LC-tank structure. However, depending on the value of the leakage inductance, the ZVS range is significantly affected. For small leakage inductance, the ZVS range is narrow meaning, any deviation in the transferred power or voltage gain may result in hard switching. If the leakage inductance is large, the ZVS range can be extended for a wider gain and power. Though, a large leakage inductor will result in higher reactive power circulation, and switch RMS current stress will increase and the efficiency will be lower. Moreover, since EV batteries have a wide range from 250–450 V for 400 V batteries and 500–900 V for 800 V batteries, optimal selection of leakage inductors requires significant effort.

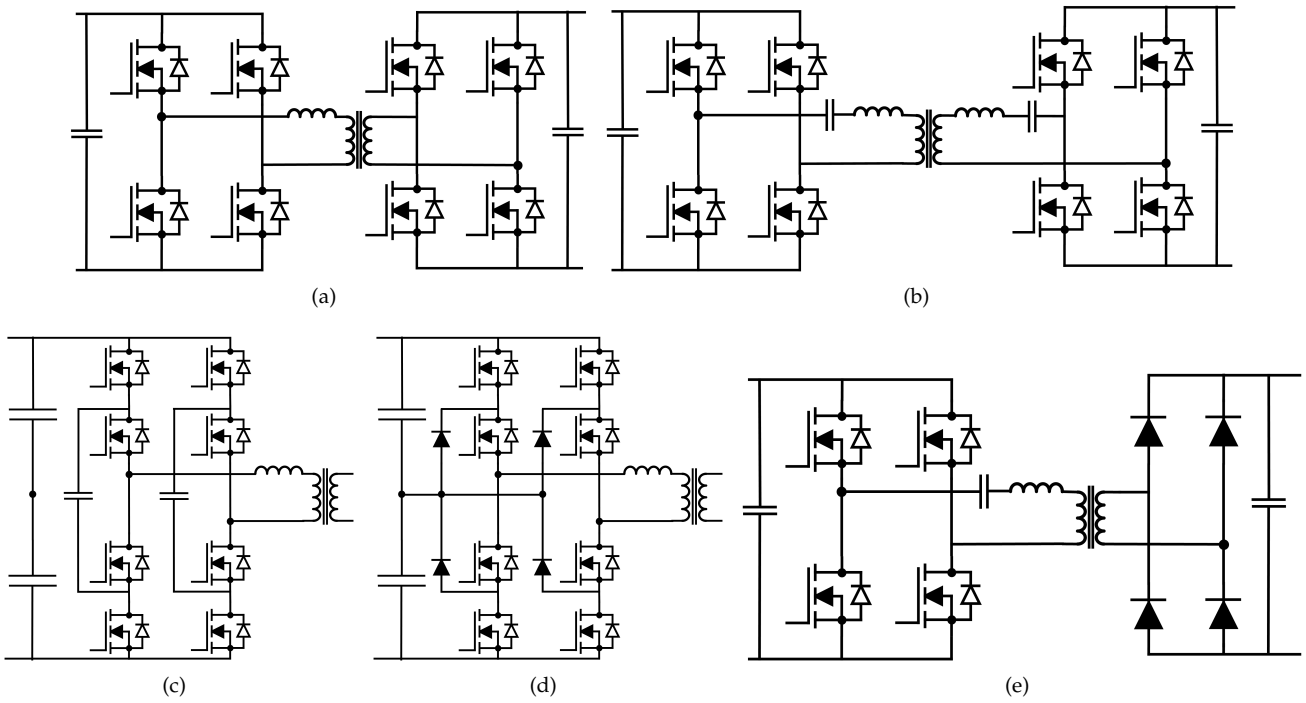

Figure 5. Isolated DC/DC converters. The secondary side of 3-level FC-DAB and NPC-DAB are omitted due to visual clarity. Similar structure as in (**c**,**d**) or (**a**) can be used to rectify the AC voltage during grid-to-vehicle (G2V) operation: (**a**) Dual Active Bridge (DAB); (**b**) CLLC converter; (**c**) 3-level flying capacitor(FC) DAB; (**d**) 3-level NPC-DAB; (**e**) LLC converter.

Another bi-directional topology is the CLLC topology [52,53]. Similar to DAB, it has eight switches and a high-frequency transformer. Two series LC resonant structure is present in both primary and secondary sides. The series LC structure acts as a band-pass filter and hence the current flowing in the whole circuit is highly sinusoidal. The elimination of high-frequency current components reduces the loss of magnetic elements. Therefore, the magnetic elements are smaller compared to DAB Moreover, compared to DAB the required leakage inductance is smaller, and hence a smaller reactive power flows through the circuit [54]. Although it is possible to achieve high efficiencies for a certain power and voltage ratio, the light load operation of CLLC is problematic. Another major element often neglected is the use of a series-connected capacitor directly on the high-frequency AC current. To increase the efficiency of CLLC converters high intrinsic quality is necessary.

This is achieved by having a high L/R ratio on the inductor and the transformer. Therefore, less capacitance is needed to achieve the same resonant frequency. However, the smaller capacitance also means higher voltage stress across the terminals of the capacitor [55]. Combined with high voltage stress coupled with high currents results in the derating and aging of the capacitance. According to [56], capacitors come second to critical power electronics system failures.

The last two bi-directional systems are 3-level flying capacitor (FC) [57] and neutral point clamped (NPC) DAB converters [58,59]. For visual clarity, the secondary sides are omitted in Figure 5c,d. For systems connected to a 400 V grid, the DC-link voltage is often set to be between 700–800 V. Therefore, including the overshoot during switching minimum 1200 V rated semiconductors are required. While SiC is already commercially available and also became feasible for the industry, GaN with high blocking voltages is still not available. If the aim is to use GaN or 650 V Si-based MOSFET, three-level topologies are also a suitable option. The 3-level FC DAB converter is such an option. It consists of eight switches on the primary side with a voltage stress of Vdc/2 on each semiconductor. Compared to 3-level NPC-DAB, FC-DAB does not need additional clamping diodes. Additionally, FC-DAB does not have the issue of voltage balancing on the neutral point. The only downside of FC-DAB is the necessity of a pre-charge circuit for the FC. Both of these topologies are quite rare since GaN technology is not still as cost-effective as SiC for a high-voltage application. Therefore, these topologies are not selected for an 800 V DC-link voltage. However, in the literature, 3-level structures are used to connect the EV chargers directly to a 3-phase medium voltage grid.

A conventional LLC converter is often employed in the literature when bi-directionality is not mandatory. Similar to the CLLC converter it has an LC resonant tank structure and the drawn current is hence highly sinusoidal [60,61]. LLC converters have excellent efficiency for the designed gain and power transfer. Due to the smaller inductor compared to DAB, a low reactive current is drawn from the system and ZVS/ZCS are achieved on primary/secondary, respectively. If designed properly, the required leakage inductor and transformer can be combined into a single magnetic element that reduces the cost/size and hence increases overall power density. LLC converter has inherent short circuit protection and a wide voltage range for light loads. However, satisfying the ZVS operation under different loading conditions for a wide voltage gain is problematic [62]. Moreover, similar to the CLLC converter, the series capacitor is subject to high voltage and current stress. Therefore, accurate lifetime calculation of the capacitor is necessary.

2.4.2. Non-Isolated DC/DC Converters

When isolation is achieved in the AC/DC stage, non-isolated DC/DC converters can be used to connect EV batteries or BESS to the DC-bus. In Figure 6, the non-isolated DC/DC converters are presented. All of the presented topologies are bi-directional but can easily be converted to uni-directional using a diode instead of active switches. Considering, the DC-link voltage is often set to 800 V, a step-down converter is required to match the EV battery voltage. From Figure 1a, conventional buck converter topology is presented. Compared to other topologies, buck converter topology is superior in terms of output side current ripple. Due to its low number of components and recent development in magnetic core materials, high power density can be achieved. However, practical buck converters designed for the EV charger often have large inductors to reduce the current ripple even further. This is because battery lifetime decreased significantly when the current ripple is high. A method to reduce the current ripple is to increase the switching frequency. Although, then the limiting factor is the switching loss of the semiconductors. To reduce the current ripple without increasing the switching frequency, interleaved DC/DC converters can be used [63]. In Figure 6b, an interleaved buck converter is presented. It consists of 2N semiconductors where N is the number of interleaved converters. The current ripple can be reduced or even eliminated completely depending on the duty cycle. Another benefit of using interleaved buck converter is to achieve redundancy and/or modularity in the system. However, a downside of having

a high number of modules is that the current sharing between the modules becomes more sensitive to duty cycle fluctuations and small variations.

If the system will be connected to a DC-bus with high voltage, then multi-level converters are a viable option. The most common topologies are NPC [64] and FC [65,66] buck converter. Both topologies have the same upside of three-level converters which are decreased voltage stress on the semiconductors, frequency doubling on the inductor (meaning less ripple or smaller inductor), high system efficiency, and improved cooling (the cooling area increased due to an increased number of semiconductors.) However, similar to NPC-AFE and NPC-DAB, the NPC topology suffers from neutral point voltage oscillations. Moreover, the FC topology requires an external precharge circuit to charge the FC to Vdc/2 at the startup [67].

Finally, when a wide voltage range is desired, a buck-boost topology may be necessary. In Figure 6e, non-inverting buck-boost topology is presented [68]. A benefit of this topology is that when operated only in buck or boost mode (two of the switches are always off), high efficiency can be achieved just as conventional buck or boost converter [69]. However, this also means two of the switches will not be used. If the operation times and thermal stress on the switches are not properly analyzed, high thermal cycling on a specific switch may result in a significant drop in reliability and lifetime. The same is true for all PWM duty-cycle controlled non-isolated DC/DC converters.

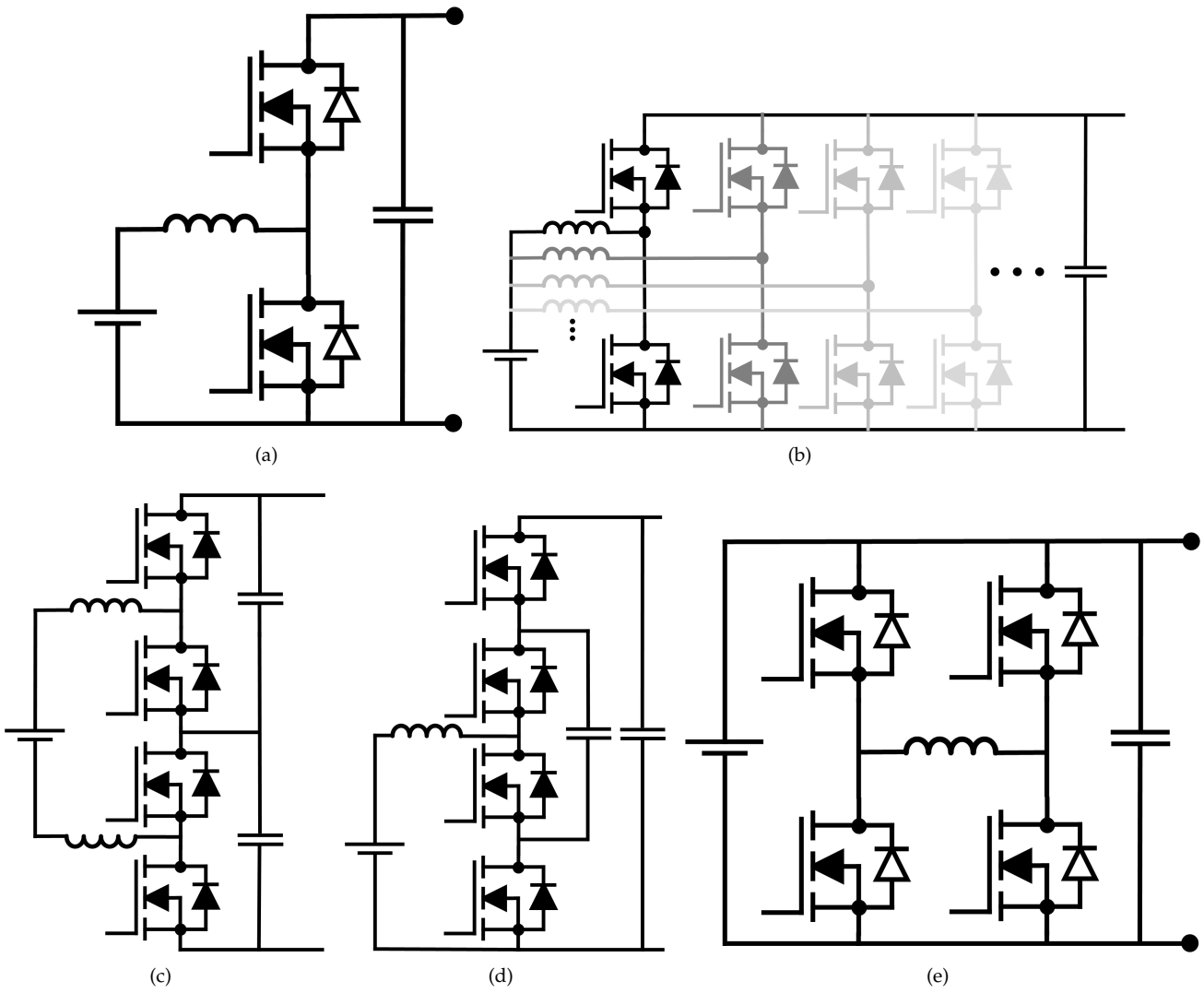

Figure 6. Non-isolated DC/DC converters: (**a**) Conventional buck converter; (**b**) Interleaved buck converter; (**c**) 3-level NPC buck converter; (**d**) 3-level FC buck converter; (**e**) Non-inverting buck-boost converter.

3. Battery Types

Lithium-ion batteries (LiBs) are a diverse array of technologies that are available on the market, including an increasing number of second-life modules that are emerging from the EV sector. The LiB cells are primarily identified by the names of their cathode materials, such as lithium cobalt oxide (LCO), lithium manganese oxide (LMO), lithium iron phosphate (LFP), lithium nickel cobalt aluminum oxide (NCA), lithium nickel manganese cobalt oxide (NMC), and lithium titanate oxide (LTO) [70]. These cells have distinct characteristics, such as cell voltage, energy density, cycle life, and cost, due to variations in their internal structure and material composition in the cathode and anode formation [71]. Furthermore, there are ongoing efforts to improve Li-ion battery cathode chemistry and material composition to deliver better performance, such as higher energy density, lower specific costs, and the removal of other bottlenecks, such as the dependence on cobalt. Table 3 contains the most important cell technology parameters. It can be observed that those containing cobalt have high power densities and energy densities, but also have disadvantages related to reduced safety and shorter longevity [72]. In contrast, those lacking cobalt (primarily LFP and LTO) have excellent cyclability and are considered quite safe, despite their low energy and power densities, with LTO being the most expensive one. LMO would be the poorest chemistry in terms of operational properties, while NMC would be the compromise chemistry that can be applied to any use or requirement [15]. Therefore, the selection and sizing of ESS must take into consideration the specific application and parameters of any LiB cell technology in the table. The optimal sizing routine is applied to find the best optimal solution, considering the performance parameters and cost of the ESS. It is found that the sizing and selection of ESS vary in terms of the total cost of ownership. Additionally, it is important to consider the lifetime parameters that affect the battery calendar and cycling lifetime, such as state of charge (SoC), C-rate, and temperature [73].

Table 3. Parameters of lithium iron phosphate (LFP), lithium nickel manganese cobalt oxide (NMC), lithium titanate oxide (LTO), lithium manganese oxide (LMO) and lithium nickel cobalt aluminum oxide (NCA) batteries using popular chemistries (based on [74–76]).

	LFP	NMC	LTO	LMO	NCA
Specific Energy (Wh/kg)	90–120	150–220	50–80	100–150	100–170
Specific Power (mAh/g)	200–1200	110–340	3000–5100	110–340	110–200
Nominal Voltage (V)	3.3	3.6	2.2	3.8	3.6
Cost (€)/kWh	260	200	500	-	166
Cycle-Life at 80% DoD and 25 °C	2000–10,000	3000–7000	2000–14,000	300–700	2000–3000
C-rate (Charge-Discharge)	1/1	0.7–1/2	1/10	0.7–1/1	0.7–1/1

Despite forecasted reductions in the cost of Li-ion battery technology, the high cost of BESS has been a topic of ongoing discussion in recent years. One potential solution to mitigate the cost of energy storage systems is the use of second-life batteries (SLBs) from electric vehicles. The primary advantage of using SLBs is demonstrated in Figure 7. With the first batch of retired EV batteries in China in 2020, the use of SLBs for stationary applications is already being tested in a number of pilot projects. The net present value of 1 kWh of SLB price ranges from 40 to 240 euros/kW based on economies of scale [77].

However, the management of large numbers of retired batteries remains unclear, and the techno-economic analysis of SLBs has become a new challenge, requiring accurate quantification of their state of health and remaining lifetime. It has been found that small variations in the second-life depth of discharge (DoD) can have a significant impact on the health of SLBs. Additionally, the cost for reusing SLB can be as low as 20 euros/kWh if vehicle diagnostic data are available to support SLB purchases [78]. Moreover, it is estimated that the available SLB will surpass the demand from the utility LiB storage as given in Figure 8 in year of 2030. This means there is a significant potential for SLB applications in the utility.

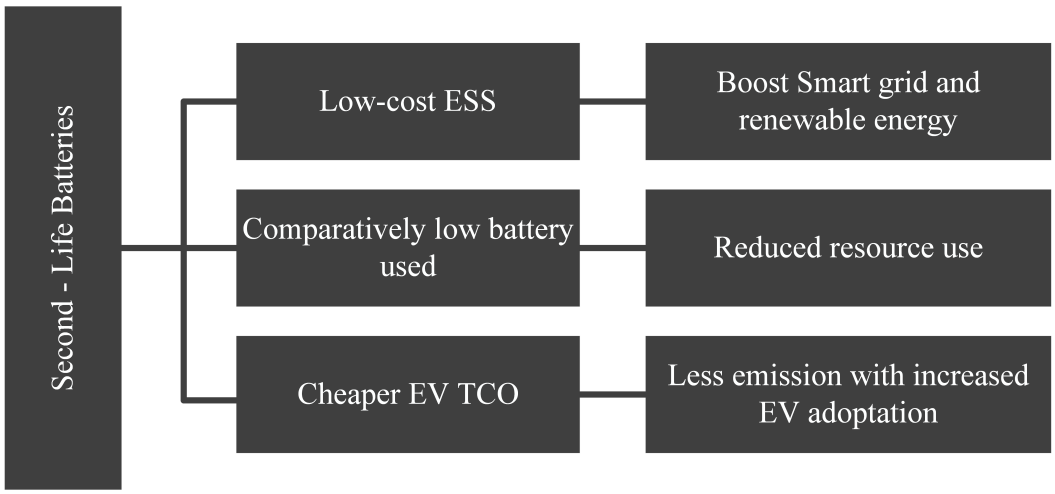

Figure 7. Advantages of second-life batteries used in stationary storage applications.

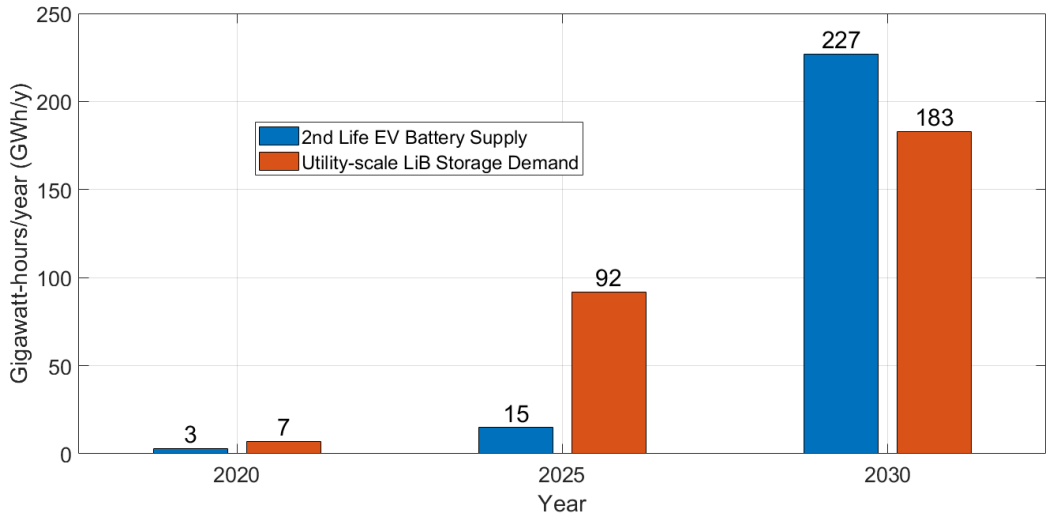

Figure 8. Estimated SLB from passenger car supply and utility demand change between 2020–2030 [79].

Finally, because of the extremely high number of SLBs, battery recycling will be a profitable business. Thus, how it is still conserved as a new value chain in ESS applications is presented in Table 4.

Table 4. Examples of battery second-life pilot and commercial projects, edited from [80,81].

OEM	Service Provider	EV Model	Capacity	Application	Country
Daimler	GETEC	Smart	13 MWh	Renewable	Germany
Nissan	-	Leaf	400 kWh/600 kWh	Renewable	Japan
Mitsubishi & PSA	EDF & Forsee Power	Peugeot Ion	N/A	Renewable	France
BMW	UC San Diego	Mini-E	160 kWh/100 kWh	Renewable	USA
BMW	Vattenfall&Bosch	ActiveE & i3	2.8 MWh/2 MWh	Renewable	Germany
BMW	Vattenfall	i3	12 kWh/50 kWh	Fast Charging	Germany
Renault	Connected Energy	Zoe	50 kWh	Fast Charging	UK

4. Failure Mechanism and Design for Reliability

Power electronics converters (PECs) are used in a variety of applications, such as wind farms and off-board chargers, and operate continuously in different environments. Any interruption in their operation can result in significant economic loss. Therefore, there is a need to meet safety requirements, such as functional safety, and to minimize the number of failures over the lifetime of the PECs.

One approach to achieving this is to consider reliability aspects in the design stage of PECs. This allows for the selection of different topologies, control systems, semiconductors, and modularity to improve reliability, in addition to efficiency, size, and cost criteria. It is important to note that reliability analysis can only be provided if the loading and environmental conditions are known. Therefore, a comprehensive understanding of semiconductors, including materials, packaging, failure mechanisms, and lifetime models is essential [82].

Even after the design of the PEC is completed, it is still possible to improve its lifetime through online methods. This can be achieved by using real-time measurements to identify any deviations from the healthy PEC baseline. This information can then be processed to further improve the lifetime of the PEC. This process of identifying potential issues is referred to as condition monitoring [83], while the actions taken to address them can be categorized as health management [84].

In this section, the materials and stages for reliability assessment and improvement of PECs are discussed in detail. The focus is on explaining the methods and techniques used to evaluate and improve the reliability of PECs throughout their lifetime, including both design-stage and online methods.

4.1. Failure Mechanism

In the SiC MOSFET, failure mechanisms can be divided into two different groups: chip-level and package-level. The reasons for these mechanisms include wear-out, electrical and mechanical shock, and thermo-mechanical loading. Typically, in PECs, wear-out mechanisms degrade the switch gradually over time, while electrical and mechanical shock may result in an instant failure [85,86]. Additionally, these degradations can be identified by monitoring certain parameters, such as ON-state voltage or thermal resistance, which are referred to as failure identifiers.

At the chip level, time-dependent dielectric breakdown (TDDB), latch-up, and hot carrier injection are well-known failure mechanisms. In TDDB, electrons are trapped and accumulated in the gate oxide layer, ultimately leading to the formation of an unwanted conduction path. The failure identifiers for TDDB are typically the gate leakage current and gate threshold voltage [87–90]. In latch-up, a high voltage slew rate (dv/dt) during the turn-OFF instant can cause the MOSFET to lose control of the drain-source/collector-emitter current [91–93]. Finally, in the hot carrier injection mechanism, electrons and holes gain kinetic energy and overcome barriers to penetrate other layers, such as the gate oxide and starting degradation mechanism [87,94].

In package-level failure mechanisms, the primary focus is on the degradation of solder interconnects, wire bonds, and die attaches. One of the most significant sources of harm

within the package is thermo-mechanical stress, caused by the difference in coefficient of thermal expansion (CTE) among the various materials. This stress can result in the formation of cracks in both solder interconnects and wire bonds.

Thermal cycling, which is caused by changes in power losses in semiconductors, is one of the major types of thermo-mechanical stress [95–97]. Solder layers play a crucial role in connecting various layers within the package, such as the die, die attach, and direct bonded copper (DBC).

The initial stage of degradation begins with the formation of cracks and voids in the solder. This leads to an increase in resistance and, over time, a decrease in the maximum heat dissipation capability. The increase in resistance also results in a rise in die temperature, which can put wire bonds at risk [98–101].

Bond wire fatigue encompasses wire bond heel crack and wire bond lift-off. As with solder interconnect fatigue, the primary cause of failure is the difference in CTE between the wire bond and the die. Wire bond heel crack arises from continuous flexion and the formation of cracks in the heel [102]. Wire bond lift, on the other hand, is caused by voids in the interconnect [103,104].

4.2. Design for Reliability

Several lifetime models have been proposed in the literature to account for the effects of junction temperature and its swing on the ultimate lifetime of semiconductors. Some important lifetime models are presented in Table 5. In these models, the variable N_f represents the number of cycles that the semiconductor is subject to a certain stress before a failure occurs. It is noteworthy that the Bayer and Semikron models incorporate additional parameters such as the wire bond diameter (D) and wire bond aspect ratio (a_r), in addition to pulse duration and heating time.

Table 5. Lifetime Models in the Literature.

Failure Model	Failure Site	Equation	Variables	Authors
Coffin-Manson	Bond-wire	$N_f = \alpha \times (\Delta T)^{-n}$	ΔT	[105]
Coffin-Manson-Arrhenius	Bond-wire	$N_f = \alpha \times (\Delta T)^{-n} \times e^{\frac{E_a}{kT_m}}$	$\Delta T_J, T_m$	[106]
Norris-Landzberg	Solder	$N_f = A \times f^{n_2} \times (\Delta T)^{-n_1} \times e^{\frac{E_a}{kT_m}}$	$\Delta T_j, T_m, f$	[86]
Bayerer	Bond-wire	$N_f = k \times (\Delta T_j)B_1 \times e^{\frac{B_2}{T_{j,max}}} \times t_{on}^{B_3} \times I^{B_4} \times V^{B_5} \times D^{B_6}$	$\Delta T_j, T_{j,max}, t_{on}, I, V, D$	[107]
SEMIKRON	Bond-wire	$N_f = A_0 \times A_1^B \times (\Delta T_j) - B \times (\Delta T_j)^{\alpha} \times (a_r)^{B_1 \Delta T_j + B_0} \times (\frac{C + (t_{on})^{\gamma}}{C + 2^{\gamma}}) \times e^{\frac{E_a}{kT_m}}$	$\Delta T_j, t_{on}, T_m$	[108]

During the design for reliability (DfR) stage, consideration is given to the reliability aspects of the design, and various metrics such as mean time to failure (MTTF) and mean time between failure (MTBF) are integrated into the optimization process. This information is of great value to designers, as it provides insight into semiconductor, capacitor, and inductor selection, the implementation of appropriate control strategies, and the use of series and parallel combinations of modules. In this stage, various types of stress, such as thermal, electrical, and mechanical, as well as environment-related factors such as humidity, are typically taken into account [109–111].

To effectively implement DfR, it is necessary to follow a stepwise procedure that begins with identifying an appropriate mission profile. For example, as presented in [112], a wind profile for a year is essential for the reliability assessment of photovoltaic energy systems in wind farms. Additionally, a solar radiation [112] and sea elevation profile [113] have been defined. In the case of electric vehicle applications, which are subject to different environments and loading scenarios, mission profiles have been defined taking into account parameters such as torque, speed, battery status, and coolant temperature [82,114,115].

As previously discussed, the main failure mechanisms in semiconductors are related to fluctuations in junction temperature. Therefore, after applying the mission profile, it is necessary to process the junction temperature resulting from cyclic thermal loads. This process includes extracting features such as dwell time, mean value, and numbers of full and half cycles, which can be accomplished through the use of counting algorithms [116]. To date, several counting algorithms have been proposed, such as peak counting and level crossing counting. However, the rain-flow counting algorithm is the most widely used [117,118]. It should be noted that the results of different counting algorithms may vary, as they are based on different definitions of temperature cycles.

In addition, components in PECs are subject to various types of stress that may change during operation. Consequently, the effects of all these stresses must be accumulated in order to estimate the final end of life (EoL) of the components. The Palmgren–Miner rule is an accumulation method that estimates EoL based on a linear equation, taking into account the stress experienced by the PECs and the maximum stress they can tolerate. In Equation (1), D represents accumulated damage, N_j represents the maximum cycles that components can endure for a specific stress level, and n_j can be calculated using counting algorithms for a specific stress level [111,119,120].

$$D = \sum_{i=1}^{m} \frac{n_j}{N_j} \tag{1}$$

4.3. Condition Monitoring and Health Maintenance

In actual operating conditions, PECs may still experience reliability issues and it is possible to improve the lifetime of semiconductors. One way to achieve this is through the implementation of a program called condition monitoring, which aims to monitor the online health status of the components and subsequently the entire system. This can be used for diagnostic and prognostic activities. Additionally, the data obtained from condition monitoring can be utilized for another program called health maintenance, which is responsible for controlling system performance and manipulating the stress experienced by semiconductors. The combination of prognostics and predictive health maintenance has led to a new research area known as prognostics and health management (PHM). One of the signals that can be used for PHM is junction temperature and its fluctuations. However, measuring this parameter can be challenging and advanced strategies may be required. Additionally, various approaches have been proposed for implementing health maintenance, and these are heavily dependent on the application. The challenges of junction temperature measurement and an overview of health maintenance approaches are discussed in this section.

Junction Temperature Estimation Methods

The initial method for determining the junction temperature involves the utilization of thermal cameras. However, this technique is not cost-effective in practical systems. Additionally, measuring the junction temperature of power modules necessitates their decoupling, further exacerbating the situation. In the alternate method, temperature sensors such as NTC or p-n diode are installed on the direct bond copper (DBC) within the package to determine the junction temperature [121,122]. However, this approach is not able to provide a fast and accurate estimation of the junction temperature due to the presence of external impedances between the sensors and the die. Additionally, the time-dependent

degradation of the device necessitates the need for calibration [116]. Additionally, some commercially available modules do not have internal temperature sensors.

Another strategy is to calculate the switching and conduction losses to input into electrothermal models [123]. This typically involves using a resistor-capacitor (RC) structure to model the thermal impedance between the junction and ambient [124,125]. A popular approach is to use one-dimensional (1-D) electrothermal simulation models. These models require less computational time, however, their accuracy is relatively low [126].

One-dimensional (1-D) models can be classified as the Cauer and Foster model, as depicted in Figure 9. The parameters for the Cauer model are calculated by considering material properties, and thus it can be inferred that each RC branch represents the internal temperature of a specific layer. However, the parameters for the Foster model are obtained through experimentation and do not provide insight into the internal temperature, but they are relatively easier to implement [127]. An attractive approach for temperature estimation in less than 100 microseconds is the use of electrical signals. This method employs parameters such as ON-state voltage, gate threshold voltage, and body diode forward voltage for temperature estimation [128,129]. One limitation of this temperature-sensitive electrical parameter (TSEP) measurement is that it only measures the average temperature of the chip and cannot accurately measure other areas such as wire bonds and solder interconnects [130,131]. Furthermore, commissioning tests are required to map electrical parameters to junction temperature, which are usually performed in controlled situations, and thus ignore device self-heating which may lead to a mismatch between the real junction temperature and the results of the commissioning tests [132]. Additionally, in actual conditions, the dynamic and static characteristics of semiconductors may change, thus regular calibration is required [101,133,134]. Moreover, measuring some TSEPs may disrupt the normal operation of the converter, such as measuring the gate threshold voltage, which can result in a reduction in the switching frequency [135].

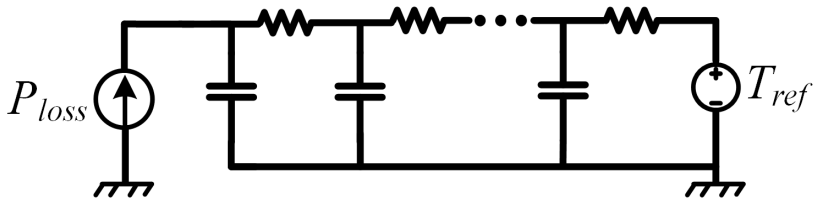

Figure 9. Cauer model representation for power electronics temperature estimation.

5. Control Methods for DC-Fast Chargers with BESS

With the recent development of computational power, control of power electronics become more sophisticated resulting in higher efficiency, high power quality, smaller component size, and even higher lifetime. In Section 4, design for reliability and PHM subjects were investigated. In addition to the passive calculation of consumed lifetime, active control methods can be applied to increase the lifetime of equal aging of different power electronic modules and battery packs. In this section, firstly the low-level control methods for both AC/DC and DC/DC stages will be presented. In addition, low-level control methods for lifetime improvement will be shared. Then, the system-level control methods including data-driven methods for improved battery/power electronics lifetime will be presented.

5.1. Low-Level Control

In Section 2, the architectures were presented. Generally, an EV charger with local BESS has two different stages, mainly the grid-connected AC/DC stage and isolated/non-isolated DC/DC stage. However, there are exceptions such as in case-3 in Figure 3 where both isolation and AC/DC rectification are achieved by matrix converters. Therefore, in this section, the control methods will be separated according to the power conversion stage.

5.1.1. AC/DC Rectifier/Inverter Low-Level Control Methods

Consider the control method presented boost type inverters (Figure 4a–c) in Figure 10. The given control method is called decoupled current control. The grid voltage and rectifier currents are converted to a synchronous frame by using a phase-locked loop (PLL) structure. It is so common practice to lock the d-axis to phase-A. Therefore, in the case where phases are balanced the Q-axis grid voltage becomes 0. According to the d-q axis active and reactive power formulation given in Equations (2) and (3), it becomes possible to control both active and reactive powers independently from each other by controlling the d and q axis current, respectively.

$$P = \frac{3}{2}(V_d I_d + \cancel{V_q I_q}) \tag{2}$$

$$Q = \frac{3}{2}(\cancel{V_q I_d} + V_d I_q) \tag{3}$$

In EV charging, the q-axis current reference is often set to operate at unity power factor since the aim is not to provide grid service. Moreover, if the converter is bi-directional V2G services can also be made by only changing the sign of the d-axis current. However, for the V2G application, the d-axis current reference should be generated from the active power equation given in Equation (2) by considering the demanded power from the grid. The additional subtraction and addition of $\omega L I_q$, $\omega L I_d$ are feed-forward terms related to the voltage drop across the inductors. Finally, the d-q reference signals are normalized and converted into actual PWM signals.

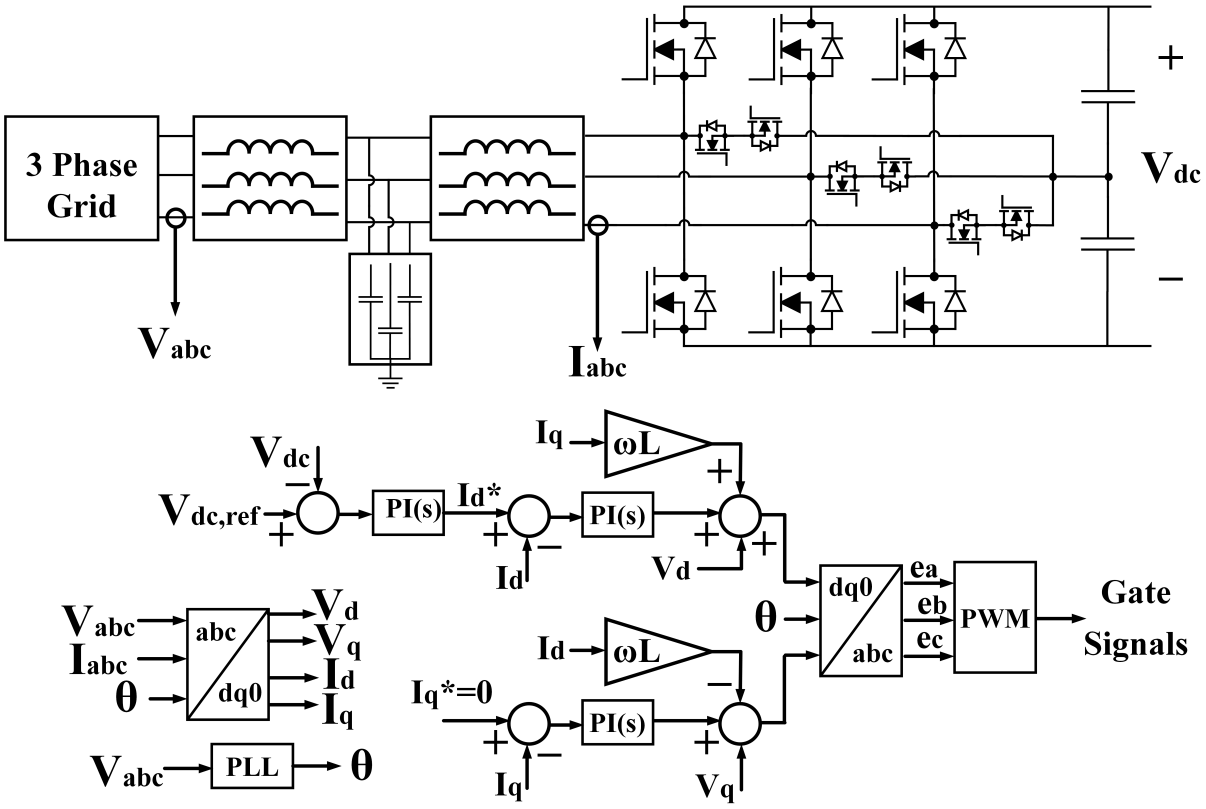

Figure 10. Decoupled current control for boost type active rectifier/inverters. The T-type inverter is given as an example. It can be any boost-type inverter.

From Figure 10, it can be seen that there are two loops. The faster inner loop is the current set-point and the slower outer loop is the DC-link voltage control. Therefore, the type of controller is also a topic needing attention. In [136], different controllers such as PI, Lead-Lag, proportional resonance, and modified proportional resonance are compared.

In [137], the phase compensated proportional controller (CPC) is presented. It is said that CPC is superior to PI controller in terms of computational burden due to the lack of park transform in CPC control. In [138], a quasi-proportional-resonant controller is proposed for a multi-functional inverter.

In [139], sliding mode control is presented for both the DC-link voltage and neutral point voltage control. The method is said to be superior to conventional methods in terms of computation since similar to CPC control it also deals with abc voltages/currents directly instead of stationary frame voltages/currents. Another important topic in AC/DC inverters is pre-charging. Assume a boost type AFE and all gate signals are pulled low. Then, the DC-link capacitors are directly connected to the grid through the body diodes of the semiconductors. Till the DC-link is fully charged ($V_{DC} \approx 560$ for 400 V_{l-l}) an in-rush current is drawn. To eliminate it startup strategies are presented in [140] for 3 phase 6 switch boost type inverter where all steps are explained in detail. Similarly, in [141] a minimum inrush start-up of a single-phase PFC is presented. Although there are control strategies, often inrush current is limited by the use of series connected resistors where they are shorted using relays after the desired voltage level is achieved.

Finally, it is important to discuss neutral point voltage balancing techniques for NPC-AFE and T-type AFE. In [142], a method called "hybrid variable virtual space vector" is proposed and said to be superior balancing properties for medium and large space vectors compared to conventional methods in [143,144].

Conventional Vienna rectifier control is almost the same as decoupled current control. The only difference is that compared to other 3-level NPC topologies, the Vienna rectifier has only one zero state. Therefore, the difference occurs for space vector PWM generation and the switching sequence [145]. In [146], a method to suppress the harmonic resonance occurring due to parasitic capacitances of transmission cables in EV chargers is presented. In [147], a voltage-oriented control is proposed. In [148], a finite set model predictive control is presented. In [149], the Vienna rectifier is modeled analytically and a sliding mode control method is described.

The fundamentals of the Swiss rectifier are presented in [150]. A PWM control strategy for the Swiss rectifier is shown in Figure 11 whose details are presented in [151]. In [152], a full bridge-based Swiss rectifier and its control for lower THD and ZVS operation is described. In [153], a non-linear control for lower THD is presented. In [154], fuzzy logic is implemented. While both fuzzy logic and PI control methods are stable, less overshoot and better dynamic response is observed for the fuzzy logic.

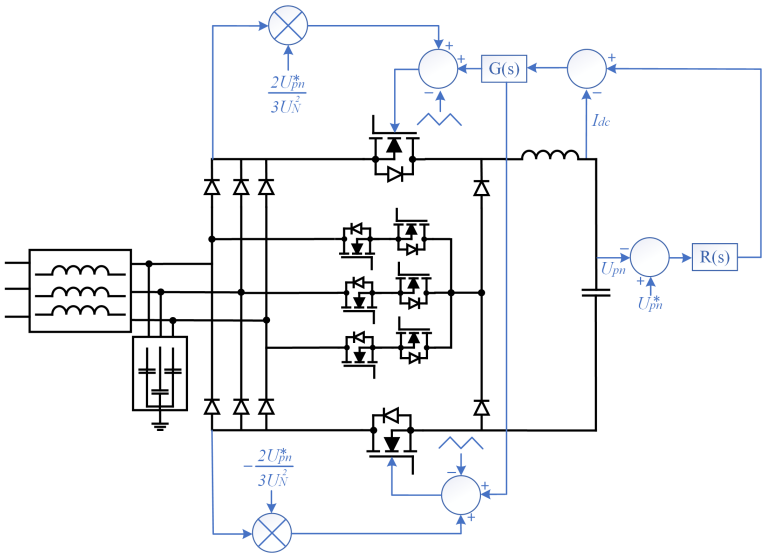

Figure 11. PWM control strategy for Swiss rectifier, edited from [151].

5.1.2. DC/DC Converter Low-Level Control Methods

In this section, the control for isolated DC/DC topologies will be presented.

1. DAB Converter:
   The DAB converter is an isolated, bidirectional topology with a low number of passive elements. The power flow direction and magnitude are controlled by the phase difference between the primary and secondary side AC voltages with the leakage inductance as the power transfer element. The most common control method is the single phase shift control (SPS) whose power equation is given in Equation (4) where P is the transferred power, V_pV_s are fundamental components of primary and secondary voltages, θ is the phase difference, ω is the angular frequency and L is the leakage inductance. An important aspect of Equation (4) is that if θ is negative, the power flow can be achieved in the opposite direction.

$$P = \frac{V_p V_s sin(\theta)}{\omega L} \tag{4}$$

   In SPS control, the primary side legs are always inversely operated and theoretically, the power flow can be achieved between $P_\theta = 90^\circ$ and zero. Moreover, the DAB converter can achieve soft switching on both sides during its operation which significantly increases the efficiency and reduces EMI and converter size. However, soft switching is only achieved for certain power levels and voltage transfer ratios. A way to increase the range of soft switching is to increase the leakage inductance but it also increases the current stress on the switches due to higher circulating current. In order to increase the light-load efficiency for a wider voltage transfer ratio, other phase shift methods such as double phase shift(DPS) or triple phase shift (TPS) are presented. By optimizing both the internal phase shifts and the voltage phase shifts, it is possible to improve efficiency, improve voltage gain, and lower transformer loss. In [155], the asymmetric phase shift (APS) method is presented and the light load efficiency is improved significantly. In [156], the double band peak current control method is used to improve the light-load efficiency by extending the ZVS range. This method limits the switching current by indirectly changing the switching frequency. In [32], modulation schemes were investigated for a 5-level DAB converter for Ultra-Wide input voltage range applications.
2. CLLC Converter:
   Compared to the DAB converter, CLLC converters have a wide output voltage range with an improved light load efficiency due to ZVS operation. In [53], dead-band control with soft-starting capability is presented. In [157], a sliding mode control method is proposed and it is said that the settling time is 0.9 ms shorter than conventional PI control strategies where the SMC settles in 1 ms. In [158], extended phase shift control (EPS) is presented and said to be superior to the pulse frequency modulation method in light loading conditions. In [159], a synchronous rectification(SR) scheme is presented resulting in a reduction in conduction losses by using a MOSFET channel instead of lossy body diodes. It is said that SR is especially critical for SiC applications since the body-diode of SiC MOSFET has a significant voltage drop across its junction.
3. LLC Converter:
   Similar to CLLC converters, LLC converters are often controlled by changing the frequency or changing the phase shift or using a combination of both methods [160]. By changing the frequency the reflected impedance is controlled [161] and by changing the phase-shift the power flow is controlled and governed by the same equation presented in Equation (4). However, a downside of the LLC converter is the light load efficiency due to increased switching frequency. To solve the issue magnetic control methods are presented in [162]. The main idea in all magnetic control methods is to intentionally saturate the external leakage inductance to achieve higher light-load efficiencies [163]. This method is similar to phase shift control since instead of changing the phase difference the inductance is changed in Equation (4). In [164], a

secondary side phase-shift method is presented, and compared to frequency control, the nominal efficiency is increased and the circulating current is decreased. In [165], an asymmetric duty cycle control is proposed and it is said to decrease the resonant current and the conduction losses of the semiconductors compared to frequency control. In [166], a hybrid PWM and pulse frequency modulation (PFM) is given. Compared to the conventional PFM method, it decreased the current spikes and enhanced output voltage regulation.

5.1.3. Low-Level Reliability Oriented Control Methods

1. Output Power Control
   In this approach, in case of any increment in junction temperature and its fluctuation, the PEC starts decreasing processing power. However, in the normal case, PEC can deliver rated power while ATC does not have any impact on normal operation [167,168]. Moreover, in PV application, by manipulating the MPPT procedure, the junction temperature of the semiconductors can be controlled [169].
2. Cooling System
   In this method, by manipulating cooling effort (i.e., cooling liquid flow rate, fan speed), the junction temperature is controlled [170–172]. In [170,171], both feed-forward and closed-loop controllers are used to increase the dynamic response of the system and minimize the temperature variation. Moreover, the ambient temperature in addition to power losses is considered for controlling the cooling system. In [172], by producing a thermal model and tuning the control system around it, junction temperature can be adjusted.
3. Switching Frequency Control
   In this approach for reducing junction temperature swings and also controlling its mean and maximum value, the switching frequency of PECs is manipulated. Basically, switching frequency changes are associated with switching loss change. To smooth temperature swings, switching frequency should be increased resulting in decreasing efficiency [123,167,173–176]. However, by using the new generation of power semiconductors such as WBG, efficiency reduction will be less in comparison with normal Si-based semiconductors [177]. Moreover, for controlling mean and maximum value, switching frequency should be decreased [167,178–181] to reduce losses in the semiconductors. However, due to the dependency of passive components on switching frequency which results in overdesign issues, this approach might not be practical.
4. Modulation Strategy
   In [182], by utilizing reactive power circulation between paralleled PECs, temperature fluctuation can be smoothed. In [183], using the condition monitoring program and estimating the remaining useful lifetime of the semiconductors, to increase the lifetime, other paralleled PECs will be requested to process more power. Authors in [184–186], implemented new space vector modulation strategies in 3-level neutral clamped PECs to change thermal distribution among power modules and thus manipulate thermal loading. In [187], via applying carrier-based modulation and redundant switching states, thermal stress can be reduced while healthy semiconductors will not experience more stress and pressure. In [188,189], by utilizing discontinuous modulation (DPWM), switching losses are decreased, and thus, thermal stress can be controlled. In [190], by switching between space vector pulse width modulation (SVPWM) and DPWM strategies in addition to manipulating switching frequency, power dissipation and consequently thermal stress are reduced.
5. Active Gate Drive Control
   Controlling gate-drive circuits is one of the hopeful methods for implementing active thermal control. The goal of this method is modifying conduction and switching power losses through controlling the turn ON and turn OFF transition and also the ON-state voltage of MOSFET/ IGBT [191]. In [192], multi-level gate-drive can smooth junction temperature fluctuation by forcing power semiconductors to work in the

saturation region. In [177], a two-step gate-driver was proposed which can control rise/fall time during switching instants in GaN HEMTs. Moreover, it was shown that the proposed approach has impacts on conduction losses in case the switching transition exceeds a certain duration. In [193–196], Wang et al. proposed an ATC method that can impact conduction losses by manipulating gate voltage and consequently drain-source resistance. However, in low gate voltage, the switch might get damaged because of a thermal runaway that can limit its applicability in a vast range of gate voltage. Moreover, in [197], a variable gate voltage methodology was employed to impact switching losses and smooth junction temperature fluctuations. In [198], by using a resistor network and switching between them, the ON/OFF switching transition can be modified according to the output load. In [199], authors could modulate switching losses via employing adaptive gate-drive in addition to controlling switching frequency. Adaptive gate drive can be implemented by changing effective gate resistance. The authors in [200], by using the gate voltage variation method and gate resistance manipulation instantaneously and also measuring junction temperature and making a comparison with the reference value, could modify switching losses and thus control junction temperature variations.

A summary of all low-level control methods for reliability is presented in Table 6.

Table 6. Low-Level Control Methods for Reliability.

TSEP	Device	Reference
Gate resistance	MOSFET/IGBT	[201–203]
Threshold voltage	MOSFET/IGBT	[204–207]
Turn-ON/OFF delay	MOSFET/IGBT	[208–214]
Rise time	MOSFET/IGBT	[212–215]
Gate drive peak current	MOSFET	[216]
Drain-source resistance	MOSFET	[217–219]
Miller capacitance	MOSFET	[220]

5.2. System-Level Reliability Oriented Control

In the industry, the OEMs are trying to achieve flexible solutions which are presented in Table 1. To achieve flexibility, modular structures are used. Therefore, different power allocation methods are investigated both in the industry and literature. In [221], a review is presented for both AC/DC and DC/DC stages for series/parallel connected module power/voltage/current sharing methods. In [222], efficiency-based droop control is presented. In [223], a resistor-based power-sharing algorithm is presented. While these methods are well developed and improved in the industry, they are not directly lifetime oriented. Having a lifetime-oriented control method reduces operational expenditure which is one of the main optimization criteria during converter sizing [15].

In [224], a reliability-oriented droop control is presented. The consumed lifetime is calculated using the rainflow counting method. The temperature swing is calculated by measuring the heatsink temperature and estimating the junction temperature using the thermal equivalent model of the converter. In [225], a similar approach is used. Considering a remaining useful life (RUL) power-sharing method, it will utilize the modules with higher RUL more and hence improve the overall lifetime. However, this also means an increase in the operational cost of the overall system. In [225], the method presented in [224] is improved to consider both lifetime and operational costs during power allocation between modules. In [226], a lifetime-oriented power sharing is applied for electric aircraft where lifetime and reliability are related to safety. Similar to [224,225] the consumed life is calculated using the rainflow algorithm. In [224–226], the consumed life is calculated considering the semiconductor lifetime. However, capacitors are also one of the main elements resulting in system failure. In [227], the lifetime calculation is made for a solid-state transformer having parallel connected DAB converters, including the capacitor lifetime.

Although reliability-oriented power-sharing methods for PECs are discussed, battery lifetime is just as important. Firstly, in [16], battery SoC and SoH online estimation methods based on a semi-empirical aging model and sigma-point Kalman filtering are presented. A method to obtain these semi-empirical aging models is to use accelerated lifetime testing as in [228]. In [229], the effect of SoC, C-rate, and temperature on the consumed life of the battery is presented. Moreover, a stochastic model is used to predict capacity loss accurately with an RMSE smaller than 1%. Therefore, it may not be the most ideal method to draw/supply the maximum power from/to the local BESS in a DC-fast charger during EV charging or off states. In [230], a method high-level for improved battery lifetime for micro-grid applications is presented. According to the authors, the proposed method increases the battery lifespan from 6.3 years to 9.2 years. The base value is obtained using a similar approach as in [224–226].

6. Power Electronics and Battery Cooling Methods

In this paper, a review of the design for reliability has been made. There are many methods to calculate the consumed life in the literature as previously presented in Table 5. Regardless of which method is used, it is always related to the magnitude and the rate of change of the semiconductor junction temperature. Moreover, from all equations in Table 5, a higher lifetime is achieved if the junction temperature is kept low and stable throughout its operation. Although a lifetime-oriented design will have better cooling, it also means either/both a larger size and a higher cooling cost. Therefore, especially for applications where high power demand is made in a short period of time such as DC-fast chargers, dangerously high junction temperatures may be reached. Similar to power electronics, batteries also require cooling to improve their lifetime and to avoid thermal runaways that may result in irreversible events [231].

6.1. Power Electronics Cooling Methods

Regardless of which architecture is selected a DC-fast charger consists of a grid-connected power filter, AC/DC AFE stage, DC/DC stage, and isolation stage. Therefore, a power electronics system cooling consists of cooling the power semiconductors, power inductors [232] and transformers [233,234] and capacitors. In [235], a review of cooling strategies is made for EV traction inverters. In Figure 12, different methods are listed with the coolant material phase and the material.

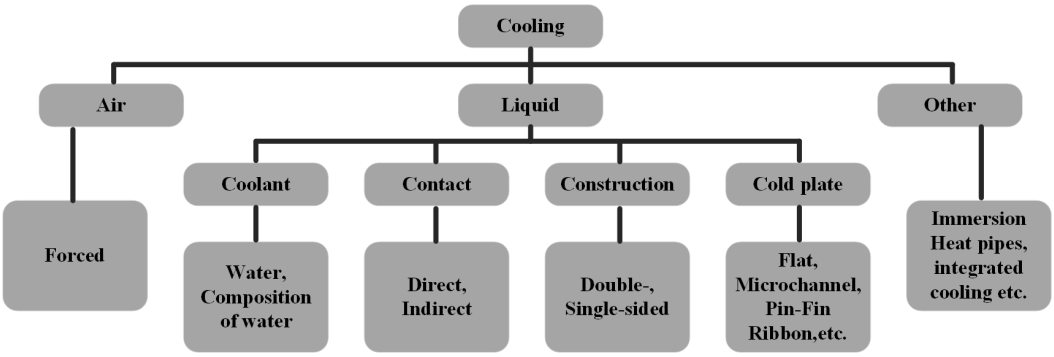

Figure 12. Different cooling methods for PE cooling [235].

In Figure 13, the cooling methods for a few industrial DC-fast charger systems are presented where the majority of the manufacturers are using liquid cooling methods with a few using forced air cooling. The advantages/disadvantages of air cooling and liquid cooling are presented in Table 7. As discussed in the introduction, the number of DC-fast charging stations will increase in the future and will be distributed. This means the chargers will be integrated into the urban areas and commercial areas ext, meaning the size of the overall system is important. Therefore, the manufacturers are choosing liquid cooling over force air cooling. Moreover, these charging systems are subject to environmental

conditions where the IP rating becomes important. Liquid cooling allows the removal of heat from enclosed systems meaning a higher IP rating can be achieved. In addition, considering the high number of chargers integrated into public spaces, reducing sound pollution is essential. Finally, a higher efficiency results in lower operational cost and less heat generation meaning a lower junction temperature oscillation resulting in a higher reliability and longer lifetime.

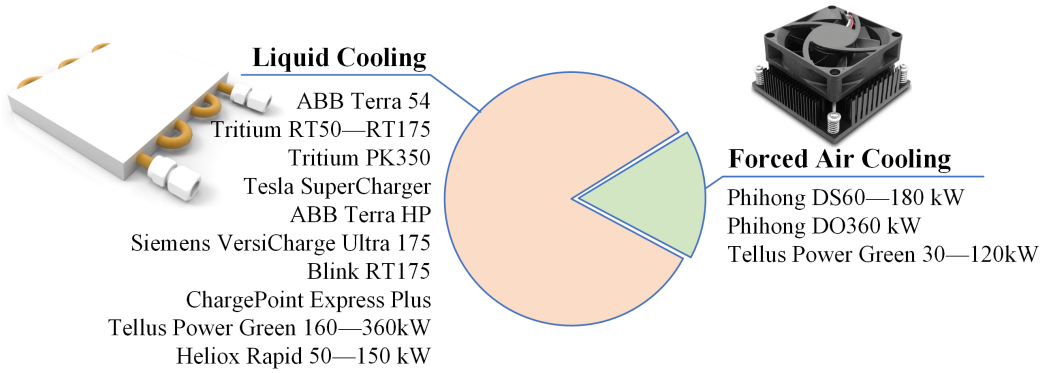

Figure 13. Type of cooling used in the commercially available industrial EV DC-fast charger systems.

Table 7. Comparison of air and liquid cooling methods.

	Advantages	Disadvantages
Air Cooling	• Low cost • Does not need additional equipment like heat-exchanger, pump,.. • Active control of fans allow control of junction temperature	• Performance depends on the environment. • Requires CFD analysis for complex systems. • Can be bulky for high-power applications. • Harder to achieve high IP ratings due to polluted air. • High operation noise. • Fan reliability effects the overall lifetime.
Liquid Cooling	• Higher efficiency • Heat removal from enclosed system is easier • Less space and lighter system • Low operation noise	• Requires CFD analysis for proper channel design • Required pumps, heat exchanger ext.

6.2. Stationary and EV Battery Cooling Methods

So far, the cooling methods for power electronics were the focus of the discussion. However, for a DC-fast charger with BESS, the cooling of batteries are just as important from the point of view of increased lifetime and reliability.

6.2.1. State-of-the-Art Cooling Methods for Local BESS and EV Batteries

Battery energy storage systems (BESS) are an important technology for renewable energy storage, as they allow excess energy to be stored and used when needed. However, one challenge with BESS is keeping the batteries at an optimal temperature to ensure their performance and longevity, particularly in challenging situations such as providing short-term power.

One of the most common methods for cooling BESS is air cooling, which uses fans or other mechanical devices to circulate air around the batteries and dissipate heat [236]. This method is relatively simple and inexpensive, but it can be less effective at cooling the batteries in high ambient temperatures or at high charge/discharge rates.

Another method for cooling BESS is liquid cooling, which uses a liquid coolant to transfer heat from the batteries to a heat exchanger [237]. This method is more effective at removing heat from the batteries, but it requires a more complex cooling system and can be more expensive to implement.

In Figure 14, different configurations for air and liquid cooling for thermal control are presented [238]. In Table 8, the advantages and disadvantages of both methods are listed.

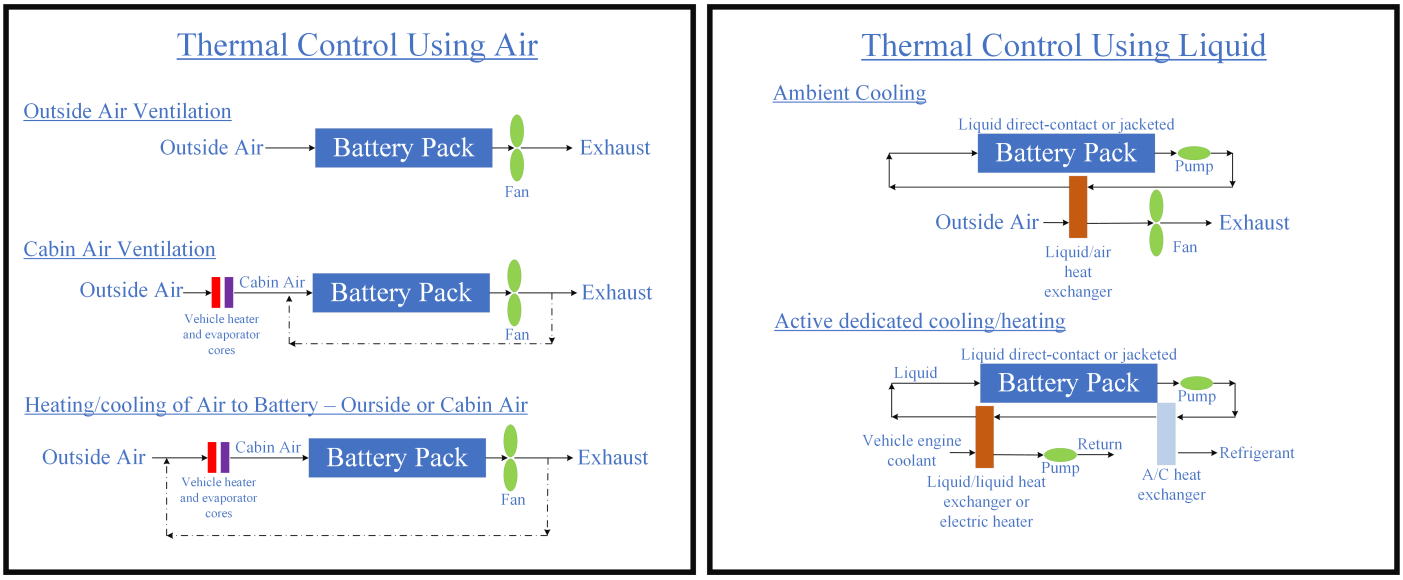

Figure 14. Different cooling methods for Battery Thermal Management.

Table 8. Advantages and Disadvantages of Using Air/Liquid for Thermal Control.

	Thermal Control Using Air	Thermal Control Using Liquid
Advantages	Waste heat released to air No separate cooling loop No leakage concern No electrical short-circuit due to leakage Simple design and lower cost Easier to maintain	Pack temperature is more uniform and thermally stable Good heat transfer capability Better thermal control Lower pumping power Lower volume Compact design
Disadvantages	Low heat transfer capability More temperature variation in the pack Might influence cabin temperature Potential of venting battery gas to cabin High blower power Blower fan noise	Additional components Higher weight Liquid conductivity can lead to isolation loss Leakage potential Higher maintenance Higher cost

A relatively newer method for cooling BESS is phase change material (PCM) cooling, which uses materials that have a high heat capacity and can absorb or release large amounts of heat without changing temperature [239]. PCM cooling can be more effective at maintaining a consistent temperature for the batteries, but it requires special PCM materials and can be challenging to implement in practice. A variation of this includes the use of phase change slurry (PCS), as a working fluid for cooling. This has the advantage of the requirement for smaller cooling circuits and associated pumps.

There are several different methods for cooling BESS, each with its own advantages and disadvantages. Air cooling is simple and inexpensive, but may not be effective at high temperatures or high charge/discharge rates. Liquid cooling is more effective, but requires a complex cooling system and can be expensive. PCM cooling can maintain a consistent temperature, but requires special materials and can be challenging to implement. Further research and development are needed to improve cooling methods for BESS and optimize their performance and longevity.

6.2.2. Smart Pre-Conditioning Methods for Battery Charging for Improved Lifetime

Pre-conditioning of battery systems typically includes the pre-heating or pre-cooling of the battery system such that the charge transfer can be maximized with minimal detrimental

effects to the batteries in terms of aging and safety [240]. These types of methods can make use of both of the thermal management circuits of the battery and also include interaction with other thermal management subsystems (such as that of the climate system) [241]. These operations can be run prior to the charging process (provided that predictive information is available), or in parallel with the charging process. Typically the higher C-Rates experienced by the battery for fast charging can lead to phenomena such as lithium plating (resulting in the loss of active material within the battery) [242]. This is most prevalent at lower temperatures and lower SOCs. As such pre-warming of the cells is desirable before fast charging can occur. Additionally, the high C-Rates over sustained periods can lead to high cell temperatures. By managing a lower starting temperature, the shorter-term requirement on the cooling circuit can be minimized. An alternative approach has also been suggested wherein the coolant is rapidly exchanged during the charging process. This method allows for the pre-conditioning of the cooling, and the high demand on the vehicle-side heating/cooling is removed [243].

Several ongoing research areas exist for the pre-conditioning for battery charging for an improved lifetime. These include:

- The development of advanced algorithms and machine learning techniques for predicting and optimizing the charging process, in order to minimize stress on the battery and maximize its capacity and longevity [244].
- The development of improved understanding of the effects of different charging protocols, such as the constant current/constant voltage (CC/CV) charging, pulse charging, and others, on the performance and lifetime of the battery [245].
- Studying the interactions between different factors that affect battery charging, such as temperature, state of charge, and charging rate, in order to develop more sophisticated models and algorithms for optimizing the charging process [246].
- Testing and evaluating smart pre-conditioning in different battery chemistries and applications, such as lithium-ion batteries for electric vehicles, stationary energy storage systems, and portable electronic devices.
- Integrating smart pre-conditioning into commercial battery charging systems, in order to demonstrate its benefits and potential for real-world applications.

There is considerable potential for further research and development in the area of smart pre-conditioning for battery charging, and this remains an open area of ongoing research.

7. Conclusions

This study presents a comprehensive examination of the current state-of-the-art advancements in DC-Fast charging systems that incorporate local battery energy storage systems (BESS). Previous research has provided a thorough review of general charging infrastructures for both on-board and off-board applications, standards, and various types of energy storage systems (ESS) and control methods (Safayatullah, 2022; Khalid, 2021; Rafi, 2021; Yilmaz, 2013). However, a detailed examination of BESS chemistries, design for reliability, reliability-oriented low/system-level control, and cooling methods had not been thoroughly explored in academic literature. This paper conducts a review of various battery chemistries and compares their cost, size, and lifetime. Additionally, it presents various low/high-level control strategies, including those for reliability and system-level reliability-oriented control, which offer OEMs lower OPEX. However, the effectiveness of these strategies is contingent on the efficiency of the cooling systems. Therefore, this paper also examines the current trends in power electronics and battery cooling technologies, including techniques such as pre-conditioning.

As potential areas for future research, this paper suggests investigating advanced methods for smart charging management strategies, with a focus on minimizing costs and maximizing the lifetime of the charging system. Additionally, the use of reliability-oriented design optimization techniques for DC-fast chargers with BESS, considering factors such as cooling, control, component selection, and sizing, may be of significant interest. Another potential area of research may be the study of second-life batteries and the practical

challenges they present in stationary BESS applications, such as CO2 emissions, safety concerns, and issues related to battery passports and multiple chemistries. Researchers and battery manufacturers may also find it beneficial to investigate the development of batteries that are designed to function effectively during both first-life and second-life operations, as this has a direct impact on the capital and operational cost. Furthermore, postponing recycling can reduce emissions, which is a pressing concern for both the present and future.

Funding: This work was supported by HiEFFICIENT project. This project has received funding from the ECSEL Joint Undertaking (JU) under grant agreement no. 101007281. The JU receives support from the European Union's Horizon 2020 research and innovation programme and Austria, Germany, Slovenia, Netherlands, Belgium, Slovakia, France, Italy, and Turkey.

Acknowledgments: The authors acknowledge HiEFFICIENT project (GA no 101007281) consortium for the support to this research. The authors also acknowledge Flanders Make for the support to our research group.

Conflicts of Interest: The authors declare no conflict of interest.

Abbreviations

The following abbreviations are used in this manuscript:

AFE	Active Front End
APS	Asymmetric Phase Shift
ATC	Active Thermal Control
BESS	Battery Energy Storage System
CAPEX	Capital Expenditure
CPC	Compensated Proportional Controller
CTE	Coefficient of Thermal Expansion
DAB	Dual Active Bridge
DBC	Direct Bonded Copper
DfR	Design for Reliability
DoD	Depth of Discharge
DPS	Double Phase Shift
DPWM	Discontinuous PWM
EMI	Electro-Magnetic Interference
EoL	End of Life
EPS	Extended Phase Shift
ESS	Energy Storage System
EV	Electric Vehicle
FC	Flying Capacitor
G2V	Grid to Vehicle
GaN	Gallium Nitrate
HEMT	High Electron Mobility Transistor
ICEV	Internal Combustion Engine Vehicle
LiB	Lithium-ion Battery
MPPT	Maximum Power Point Tracker
MTBF	Mean Time between Failure
MTTF	Mean Time to Failure
NPC	Neutral Point Clamped
NTC	Negative Temperature Coefficient
OEM	Original Equipment Manufacturer
OPEX	Operational Expenditure

PCM	Phase Change Material
PCS	Phase Change Slurry
PEC	Power Electronics Converter
PFC	Power Factor Corrector
PFM	Pulse Frequency Modulation
PHM	Prognostics and Health Management
PI	Proportional Integral
PLL	Phase Locked Loop
RMS	Root Mean Square
RUL	Remaining Useful Life
SiC	Silicon Carbide
SLB	Second Life Battery
SMC	Sliding Mode Controller
SoC	State of Charge
SoH	State of Health
SPS	Single Phase Shift
SR	Synchronous Rectification
SVPWM	Space Vector PWM
TDDB	Time Dependent Dielectric Breakdown
THD	Total Harmonic Distortion
TPS	Triple Phase Shift
TSEP	Temperature Sensitive Electrical Parameter
V2G	Vehicle to Grid
WBG	Wide Band Gap
ZCS	Zero Current Switching
ZVS	Zero Voltage Switching

References

1. EV Charging Infrastructure Incentives in Europe 2022. Available online: https://blog.evbox.com/ev-charging-infrastructure-incentives-eu (accessed on 17 November 2022).
2. When Fossil Fuels Run Out, What Then? Available online: https://mahb.stanford.edu/library-item/fossil-fuels-run/ (accessed on 17 November 2022).
3. Emissions by Sector. Available online: https://ourworldindata.org/emissions-by-sector (accessed on 17 November 2022).
4. Pevec, D.; Babic, J.; Carvalho, A.; Ghiassi-Farrokhfal, Y.; Ketter, W.; Podobnik, V. Electric Vehicle Range Anxiety: An Obstacle for the Personal Transportation (R)evolution? In Proceedings of the 2019 4th International Conference on Smart and Sustainable Technologies (SpliTech), Split, Croatia, 18–21 June 2019.
5. Electric Car Range and Affordability: Is There a Magic Combo? Available online: https://insideevs.com/news/380555/ev-range-ev-market-evolution-exposed/ (accessed on 17 November 2022).
6. Yilmaz, M.; Krein, P.T. Review of battery charger topologies, charging power levels, and infrastructure for plug-in electric and hybrid vehicles. *IEEE Trans. Power Electron.* **2013**, *28*, 2151–2169. [CrossRef]
7. Johnson, S.C.; Papageorgiou, D.J.; Mallapragada, D.S.; Deetjen, T.A.; Rhodes, J.D.; Webber, M.E. Evaluating rotational inertia as a component of grid reliability with high penetrations of variable renewable energy. *Energy* **2019**, *180*, 258–271. [CrossRef]
8. The Duck Curve on California's Grid Will Encourage Innovation and Creative Thinking. Available online: https://www.greentechmedia.com/articles/read/californias-duck-curve-will-encourage-innovation (accessed on 17 November 2022).
9. Khalid, M.R.; Khan, I.A.; Hameed, S.; Asghar, M.S.J.; Ro, J.S. A Comprehensive Review on Structural Topologies, Power Levels, Energy Storage Systems, and Standards for Electric Vehicle Charging Stations and Their Impacts on Grid. *IEEE Access* **2021**, *9*, 128069–128094. [CrossRef]
10. Kriukov, A.; Gavrilas, M.; Ivanov, O.; Grigoras, G.; Neagu, B.C.; Scarlatache, F. Novel Decentralized Voltage-Centered EV Charging Control Algorithm Using DSRC System in Low Voltage Distribution Networks. *IEEE Access* **2021**, *9*, 164779–164800. [CrossRef]
11. Hua, L.; Wang, J.; Zhou, C. Adaptive electric vehicle charging coordination on distribution network. *IEEE Trans. Smart Grid* **2014**, *5*, 2666–2675. [CrossRef]
12. Bai, S.; Du, Y.; Lukic, S. Optimum design of an EV/PHEV charging station with DC bus and storage system. In Proceedings of the 2010 IEEE Energy Conversion Congress and Exposition, Atlanta, GA, USA, 12–16 September 2010; pp. 1178–1184. [CrossRef]
13. Rafi, M.A.H.; Bauman, J. A Comprehensive Review of DC Fast-Charging Stations with Energy Storage: Architectures, Power Converters, and Analysis. *IEEE Trans. Transp. Electrif.* **2021**, *7*, 345–368. [CrossRef]
14. Utility-Scale Battery Storage. Available online: https://atb.nrel.gov/electricity/2021/utility-scale_battery_storage (accessed on 17 November 2022).

15. Hasan, M.M.; Berseneff, B.; Meulenbroeks, T.; Cantero, I.; Chakraborty, S.; Geury, T.; Hegazy, O. A Multi-Objective Co-Design Optimization Framework for Grid-Connected Hybrid Battery Energy Storage Systems: Optimal Sizing and Selection of Technology. *Energies* **2022**, *15*, 5355 . [CrossRef]
16. Laurin, A.; Heiries, V.; Montaru, M. State-of-Charge and State-of-Health online estimation of Li-ion battery for the More Electrical Aircraft based on semi-empirical ageing model and Sigma-Point Kalman Filtering. In Proceedings of the 2021 Smart Systems Integration (SSI), Grenoble, France, 27–29 April 2021; pp. 20–23. [CrossRef]
17. Hasan, M.M.; Hasan, M.; Chakraborty, S.; Baghdadi, M.E.; Razzak, A. Evaluation of Failure Trends on a PID-Controlled Synchronous Buck Converter based Battery Charging Controller. In Proceedings of the 2020 IEEE International Conference on Power Electronics, Smart Grid and Renewable Energy (PESGRE2020), Cochin, India, 2–4 January 2020; pp. 1–6.
18. Gonzalez-Hernando, F.; San-Sebastian, J.; Arias, M.; Rujas, A.; Iannuzzo, F. Discontinuous PWM for Online Condition Monitoring of SiC Power Modules. *IEEE J. Emerg. Sel. Top. Power Electron.* **2020**, *8*, 323–330. [CrossRef]
19. Safayatullah, M.; Elrais, M.T.; Ghosh, S.; Rezaii, R.; Batarseh, I. A Comprehensive Review of Power Converter Topologies and Control Methods for Electric Vehicle Fast Charging Applications. *IEEE Access* **2022**, *10*, 40753–40793. .. [CrossRef]
20. Tu, H.; Feng, H.; Srdic, S.; Lukic, S. Extreme Fast Charging of Electric Vehicles: A Technology Overview. *IEEE Trans. Transp. Electrif.* **2019**, *5*, 861–878. [CrossRef]
21. How Long Does it Take to Charge an Electric Vehicle? Available online: https://carge.co/blog/charging/ev-battery-charging-time (accessed on 17 November 2022).
22. Most of The EV Industry to Shift to 800 Volts by 2025, Report Says. Available online: https://insideevs.com/news/580829/ev-industry-shifting-to-800-volt-2025/ (accessed on 17 November 2022).
23. Menon, U.; Panda, D. Design and Evaluation of Electric Bus Systems for Metropolitan Cities. *Int. J. Mech. Eng.* **2020**, *7*, 16–23. [CrossRef]
24. Terra HP Charger-Up to 350 kW. Available online: https://new.abb.com/ev-charging/high-power-charging (accessed on 17 November 2022).
25. Terra 54 CJG. Available online: https://new.abb.com/ev-charging/dc-fast-chargers/terra-54-cjg (accessed on 17 November 2022).
26. Ultra 175 DC Charger. Available online: https://assets.new.siemens.com/siemens/assets/api/uuid:1777fe11-fa33-45f6-a339-bd522d5f6059/sidst40085004auslores.pdf (accessed on 17 November 2022).
27. EVBox Troniq Modular. Available online: https://evbox.com/en/ev-chargers/troniq-modular (accessed on 17 November 2022).
28. Supercharger. Available online: https://www.tesla.com/en_eu/supercharger (accessed on 17 November 2022).
29. Heliox Rapid 50–300 kW. Available online: https://www.heliox-energy.com/products/rapid-150kw-modular (accessed on 17 November 2022).
30. Electric Vehicle Conductive Charging System—Part 23: DC Electric Vehicle Charging Station. Available online: https://www.iecee.org/dyn/www/f?p=106:49:0::::FSP_STD_ID:6032 (accessed on 17 November 2022).
31. Safety of Power Converters for Use in Photovoltaic Power Systems—Part 1: General Requirements. Available online: https://webstore.iec.ch/publication/6470 (accessed on 17 November 2022).
32. Bezerra, P.A.; Krismer, F.; Burkart, R.M.; Kolar, J.W. Bidirectional Isolated Non-Resonant DAB DC-DC Converter for Ultra-Wide Input Voltage Range Applications. In Proceedings of the 2014 International Power Electronics and Application Conference and Exposition, Shanghai, China, 5–8 November 2014; pp. 1038–1044. [CrossRef]
33. Design Guide: TIDA-010054 Bidirectional, Dual Active Bridge Reference Design for Level 3 Electric Vehicle Charging Stations, 2022. Available online: https://www.ti.com/tool/TIDA-010054 (accessed on 17 November 2022).
34. Kumar, R.; Singh, B. Matrix converter based three phase isolated ev charger with direct power control. In Proceedings of the 2020 IEEE International Conference on Power Electronics, Drives and Energy Systems (PEDES), Jaipur, India, 16–19 December 2020. [CrossRef]
35. Jahnes, M.; Zhou, L.; Eull, M.; Wang, W.; Preindl, M. Design of a 22kW Transformerless EV Charger With V2G Capabilities and Peak 99.5% Efficiency. *IEEE Trans. Ind. Electron.* **2022**, *70*, e3192697. [CrossRef]
36. Rasool, H.; Verbrugge, B.; Zhaksylyk, A.; Tran, T.M.; Baghdadi, M.E.; Geury, T.; Hegazy, O. Design Optimization and Electro-Thermal Modeling of an Off-Board Charging System for Electric Bus Applications. *IEEE Access* **2021**, *9*, 84501–84519. [CrossRef]
37. Mortezaei, A.; Abdul-Hak, M.; Simoes, M.G. A Bidirectional NPC-based Level 3 EV Charging System with Added Active Filter Functionality in Smart Grid Applications. In Proceedings of the 2018 IEEE Transportation Electrification Conference and Expo (ITEC), Long Beach, CA, USA, 13–15 June 2018; pp. 1065–1070. [CrossRef]
38. Schweizer, M.; Kolar, J.W. Design and implementation of a highly efficient three-level T-type converter for low-voltage applications. *IEEE Trans. Power Electron.* **2013**, *28*, 899–907. [CrossRef]
39. Bolsi, P.C.; Prado, E.O.; Sartori, H.C.; Lenz, J.M.; Pinheiro, J.R. LCL Filter Parameter and Hardware Design Methodology for Minimum Volume Considering Capacitor Lifetimes. *Energies* **2022**, *15*. [CrossRef]
40. Liu, Q.; Peng, L.; Kang, Y.; Tang, S.; Wu, D.; Qi, Y. A novel design and optimization method of an LCL filter for a shunt active power filter. *IEEE Trans. Ind. Electron.* **2014**, *61*, 4000–4010. [CrossRef]
41. Yu, L.; Peng, X.; Gao, S. Voltage-balancing strategy for three-level neutral point clamped cascade converter under sequence pulse modulation. *Energies* **2019**, *12*. [CrossRef]

42. Kolar, J.W.; Drofenik, U.; Zach, F.C. VIENNA rectifier II—A novel single-stage high-frequency isolated three-phase PWM rectifier system. *IEEE Trans. Ind. Electron.* **1999**, *46*, 674–691. [CrossRef]
43. Soeiro, T.B.; Friedli, T.; Kolar, J.W. Swiss rectifier—A novel three-phase buck-type PFC topology for Electric Vehicle battery charging. In Proceedings of the 2012 Twenty-Seventh Annual IEEE Applied Power Electronics Conference and Exposition (APEC), Orlando, FL, USA, 5–9 February 2012; pp. 2617–2624. [CrossRef]
44. Schrittwieser, L.; Leibl, M.; Haider, M.; Thony, F.; Kolar, J.W.; Soeiro, T.B. 99.3% Efficient three-phase buck-type all-SiC SWISS Rectifier for DC distribution systems. *IEEE Trans. Power Electron.* **2017**, *34*, 2173–2178. [CrossRef]
45. Monteiro, V.; Pinto, J.G.; Afonso, J.L. Operation Modes for the Electric Vehicle in Smart Grids and Smart Homes: Present and Proposed Modes. *IEEE Trans. Veh. Technol.* **2016**, *65*, 1007–1020. [CrossRef]
46. Naghibi, B.; Masoum, M.A.S.; Deilami, S. Effects of V2H Integration on Optimal Sizing of Renewable Resources in Smart Home Based on Monte Carlo Simulations. *IEEE Power Energy Technol. Syst. J.* **2018**, *5*, 73–84. [CrossRef]
47. Grid-Connected Electric Buses Could Displace Diesels Electric Bus Batteries Could Earn Payments with Local Grid Operator While Providing Health Benefits to Children. Available online: https://spectrum.ieee.org/gridconnected-electric-buses-could-displace-diesels (accessed on 17 November 2022).
48. Schrittwieser, L.; Leibl, M.; Kolar, J.W. 99% Efficient isolated three-phase matrix-type DAB buck-boost PFC rectifier. *IEEE Trans. Power Electron.* **2020**, *35*, 138–157. [CrossRef]
49. Zhang, L.; Zheng, Z.; Lou, X. A review of WBG and Si devices hybrid applications. *Chin. J. Electr. Eng.* **2021**, *7*, 1–20. [CrossRef]
50. Hoek, H.V.; Neubert, M.; Doncker, R.W.D. Enhanced modulation strategy for a three-phase dual active bridge—Boosting efficiency of an electric vehicle converter. *IEEE Trans. Power Electron.* **2013**, *28*, 5499–5507. [CrossRef]
51. Hou, N.; Li, Y.W. Overview and Comparison of Modulation and Control Strategies for a Nonresonant Single-Phase Dual-Active-Bridge DC-DC Converter. *IEEE Trans. Power Electron.* **2020**, *35*, 3148–3172. [CrossRef]
52. Chen, W.; Rong, P.; Lu, Z. Snubberless bidirectional DC-DC converter with new CLLC resonant tank featuring minimized switching loss. *IEEE Trans. Ind. Electron.* **2010**, *57*, 3075–3086. [CrossRef]
53. Jung, J.H.; Kim, H.S.; Ryu, M.H.; Baek, J.W. Design methodology of bidirectional CLLC resonant converter for high-frequency isolation of DC distribution systems. *IEEE Trans. Power Electron.* **2013**, *28*, 1741–1755. [CrossRef]
54. Liu, Y.; Du, G.; Wang, X.; Lei, Y. Analysis and design of high-efficiency bidirectional GaN-based CLLC resonant converter. *Energies* **2019**, *12*, 3859. [CrossRef]
55. Bidirectional CLLLC Resonant Dual Active Bridge (DAB) Reference Design for HEV/EV Onboard Charger. Available online: https://www.ti.com/lit/ug/tidueg2c/tidueg2c.pdf?ts=1669172223698 (accessed on 17 November 2022).
56. Chakraborty, S.; Hasan, M.M.; Tran, D.D.; Jaman, S.; Bossche, P.V.D.; Baghdadi, M.E.; Hegazy, O. Reliability Assessment of a WBG-based Interleaved Bidirectional HV DC/DC Converter for Electric Vehicle Drivetrains. In Proceedings of the 2020 15th International Conference on Ecological Vehicles and Renewable Energies (EVER), Monte-Carlo, Monaco, 10–12 September 2020. [CrossRef]
57. Higa, H.; Itoh, J.I. Derivation of operation mode for flying capacitor topology applied to three-level DAB converter. In Proceedings of the 2015 IEEE 2nd International Future Energy Electronics Conference (IFEEC), Taipei, Taiwan, 1–4 November 2015. [CrossRef]
58. Feng, H.; Teng, F.; Montes, O.A.; Awal, M.A.; Bipu, M.R.H.; Husain, I.; Lukic, S. Passive Capacitor Voltage Balancing of SiC-Based Three-Level Dual-Active-Bridge Converter Using Hybrid NPC-Flying Capacitor Structure. *IEEE Trans. Power Electron.* **2022**, *37*, 4183–4194. [CrossRef]
59. Awal, M.A.; Bipu, M.R.H.; Montes, O.A.; Feng, H.; Husain, I.; Yu, W.; Lukic, S. Capacitor Voltage Balancing for Neutral Point Clamped Dual Active Bridge Converters. *IEEE Trans. Power Electron.* **2020**, *35*, 11267–11276. . [CrossRef]
60. Designing an LLC Resonant Half-Bridge Power Converter. Available online: https://www.ti.com/seclit/ml/slup263/slup263.pdf (accessed on 17 November 2022).
61. Resonant LLC Converter: Operation and Design. Available online: https://www.infineon.com/dgdl/Application_Note_Resonant+LLC+Converter+Operation+and+Design_Infineon.pdf?fileId=db3a30433a047ba0013a4a60e3be64a1 (accessed on 17 November 2022).
62. Huber, J.E.; Minibock, J.; Kolar, J.W. Generic Derivation of Dynamic Model for Half-Cycle DCM Series Resonant Converters. *IEEE Trans. Power Electron.* **2018**, *33*, 4–7. [CrossRef]
63. Alharbi, M.A.; Alcaide, A.M.; Dahidah, M.; Montero-Robina, P.; Ethni, S.; Pickert, V.; Leon, J.I. Rotating Phase-Shedding for Interleaved DC-DC Converter-Based EVs Fast DC Chargers. *IEEE Trans. Power Electron.* **2022**, *38*, 1901–1909. [CrossRef]
64. Carstensen, C.; Biela, J. A Three-Level Buck Converter with a Wide Voltage Operation Range for Hardware-in-the-Loop Test Systems. *IEEE Trans. Power Electron.* **2016**, *31*, 6176–6191. [CrossRef]
65. Song, L.; Duan, S.; Wang, T.; Liu, X. A Simplified Flying Capacitor Voltage Control Strategy for Hybrid Clamped Three-Level Boost Converter in Photovoltaic System. *IEEE Trans. Ind. Electron.* **2022**, *69*, 8004–8014. [CrossRef]
66. Qian, W.; Cha, H.; Peng, F.Z.; Tolbert, L.M. 55-kW variable 3X DC-DC converter for plug-in hybrid electric vehicles. *IEEE Trans. Power Electron.* **2012**, *27*, 1668–1678. [CrossRef]
67. Keyhani, H.; Toliyat, H.A. Flying-capacitor boost converter. In Proceedings of the 2012 Twenty-Seventh Annual IEEE Applied Power Electronics Conference and Exposition (APEC), Orlando, FL, USA, 5–9 February 2012; pp. 2311–2318. [CrossRef]
68. Schaltz, E.; Rasmussen, P.O.; Khaligh, A. Non-Inverting Buck-Boost Converter for Fuel Cell Applications. In Proceedings of the 2008 34th Annual Conference of IEEE Industrial Electronics, Orlando, FL, USA, 10–13 November 2008. [CrossRef]

69. Rao, A.V.; Guruswamy, K.P. Analysis, Design and Simulation of Non-Inverting Buck-Boost DC-DC Converter for Battery Charging. In Proceedings of the 2021 International Conference on Disruptive Technologies for Multi-Disciplinary Research and Applications (CENTCON), Bengaluru, India, 19–21 November 2021; pp. 79–84. [CrossRef]
70. Ayuso, P.; Beltran, H.; Segarra-Tamarit, J.; Pérez, E. Optimized profitability of LFP and NMC Li-ion batteries in residential PV applications. *Math. Comput. Simul.* **2021**, *183*, 97–115. [CrossRef]
71. Tran, M.K.; Dacosta, A.; Mevawalla, A.; Panchal, S.; Fowler, M. Comparative study of equivalent circuit models performance in four common lithium-ion batteries: LFP, NMC, LMO, NCA. *Batteries* **2021**, *7*, 51. [CrossRef]
72. Murdock, B.E.; Toghill, K.E.; Tapia-Ruiz, N. A Perspective on the Sustainability of Cathode Materials used in Lithium-Ion Batteries. *Adv. Energy Mater.* **2021**, *11*, e202102028. [CrossRef]
73. Baloyi, T.; Chowdhury, S. Sizing and selection of battery energy storage system for time of use arbitrage in a commercial building in South Africa. In Proceedings of the 2021 IEEE PES/IAS PowerAfrica, Nairobi, Kenya, 23–27 August 2021. [CrossRef]
74. BU-205: Types of Lithium-Ion. Available online: https://batteryuniversity.com/article/bu-205-types-of-lithium-ion (accessed on 17 November 2022).
75. Electricity Storage and Renewables: Costs and Markets to 2030. Available online: https://www.irena.org/publications/2017/oct/electricity-storage-and-renewables-costs-and-markets (accessed on 17 November 2022).
76. Li-Ion Batteries for Mobility and Stationary Storage Applications. Available online: https://publications.jrc.ec.europa.eu/repository/handle/JRC113360 (accessed on 17 November 2022).
77. Shahjalal, M.; Roy, P.K.; Shams, T.; Fly, A.; Chowdhury, J.I.; Ahmed, M.R.; Liu, K. A review on second-life of Li-ion batteries: Prospects, challenges, and issues. *Energy* **2022**, *241*, 122881. [CrossRef]
78. Rybarik, M.; Bracinik, P.; Kajanova, M. Overview of the Usability of Second-Life Batteries in Smart Distribution Grids. In Proceedings of the 2022 Elektro (Elektro), Krakow, Poland, 23–26 May 2022. [CrossRef]
79. Second-life EV batteries: The newest value pool in energy storage. Available online: https://www.mckinsey.com/industries/automotive-and-assembly/our-insights/second-life-ev-batteries-the-newest-value-pool-in-energy-storage (accessed on 17 November 2022).
80. Reinhardt, R.; Christodoulou, I.; Gassó-Domingo, S.; García, B.A. Towards sustainable business models for electric vehicle battery second use: A critical review. *J. Environ. Manag.* **2019**, *245*, 432–446. [CrossRef]
81. Zhu, J.; Mathews, I.; Ren, D.; Li, W.; Cogswell, D.; Xing, B.; Sedlatschek, T.; Kantareddy, S.N.R.; Yi, M.; Gao, T.; et al. End-of-life or second-life options for retired electric vehicle batteries. *Cell Rep. Phys. Sci.* **2021**, *2*, e100537. [CrossRef]
82. Chakraborty, S. Real-Life Mission Profile Oriented Lifetime Estimation of a SiC Interleaved Bidirectional HV DC/DC Converter for Electric Vehicle Drivetrains. *IEEE J. Emerg. Sel. Top. Power Electron.* **2021**, *10*, 5142–5167. [CrossRef]
83. Xiang, D.; Ran, L.; Tavner, P.; Yang, S.; Bryant, A.; Mawby, P. Condition monitoring power module solder fatigue using inverter harmonic identification. *IEEE Trans. Power Electron.*, **2011**, *27*, 235–247. [CrossRef]
84. Degrenne, N.; Ewanchuk, J.; David, E.; Boldyrjew, R.; Mollov, S. A review of prognostics and health management for power semiconductor modules. In Proceedings of the Annual Conference of the Prognostics and Health Management Society, PHM, Beijing, China, 21–23 October 2015; pp. 242–252.
85. Hanif, A.; Yu, Y.; Devoto, D.; Khan, F. A Comprehensive Review Toward the State-of-the-Art in Failure and Lifetime Predictions of Power Electronic Devices. *IEEE Trans. Power Electron.* **2018**, *34*, 4729–4746. [CrossRef]
86. Kovačević, I.; Drofenik, U.; Kolar, J. New physical model for lifetime estimation of power modules. In Proceedings of the International Power Electronics Conference—ECCE Asia, IPEC, Sapporo, Japan, 21–24 June 2010; pp. 2106–2114. [CrossRef]
87. Halim, M.; Buniyamin, N.; Naoe, N.; Rosman, M. An Overview of Data-Driven and Model-Driven Based Prognostics Techniques for Power Modules. In Proceedings of the 4th International Conference on Electrical, Electronics and System Engineering, ICEESE, Kuala Lumpur, Malaysia, 8–9 November 2018; pp. 34–39. [CrossRef]
88. Faure, D.; Bru, D.; Ali, C.; Giret, C.; Christensen, K. Gate oxide breakdown characterization on 0.13um CMOS technology. *Microelectron. Reliab.* **2003**, *43*, 1519–1523. [CrossRef]
89. Nasrin, M.; Khan, F.; Alam, M. Quantifying device degradation in live power converters using SSTDR assisted impedance Matrix. *IEEE Trans. Power Electron.* **2013**, *29*, 3116–3131. [CrossRef]
90. Lelis, A.; Green, R.; Habersat, D.; El, M. Basic mechanisms of threshold-voltage instability and implications for reliability testing of SiC MOSFETs. *IEEE Trans. Electron. Devices* **2014**, *62*, 316–323. [CrossRef]
91. Wu, W. SEM investigation on IGBT latch-up failure. In Proceedings of the 2001 6th International Conference on Solid-State and Integrated Circuit Technology. Proceedings (Cat. No. 01EX443), Shanghai, China, 22–25 October 2001; pp. 1040–1042. [CrossRef]
92. Singh, P. Power MOSFET failure mechanisms. In Proceedings of the 26th Annual International Telecommunications Energy Conference, Chicago, IL, USA, 19–23 September 2004; pp. 499–502. [CrossRef]
93. Patil, N.; Celaya, J.; Das, D.; Goebel, K.; Pecht, M. Precursor parameter identification for insulated gate bipolar transistor (IGBT) prognostics. *IEEE Trans. Reliab.* **2009**, *58*, 271–276. [CrossRef]
94. Ma, J. *Study of Gate Oxide Breakdown and Hot Electron Effect on Cmos Circuit Performances*; University of Central Florida: Orlando, FL, USA, 2009.
95. Xiong, Y.; Cheng, X.; Shen, Z.; Mi, C.; Wu, H.; Garg, V. Prognostic and warning system for power-electronic modules in electric, hybrid electric, and fuel-cell vehicles. *IEEE Trans. Ind. Electron.* **2008**, *55*, 2268–2276. [CrossRef]

96. Ramminger, S.; Seliger, N.; Wachutka, G. Reliability model for Al wire bonds subjected to heel crack failures. *Microelectron. Reliab.* **2000**, *40*, 1521–1525. [CrossRef]
97. Lutz, J.; Schlangenotto, H.; Scheuermann, U.; Doncker, R.D. *Semiconductor Power Devices*; Springer: Berlin/Heidelberg, Germany, 2011. [CrossRef]
98. Testa, A. Stress analysis and lifetime estimation on power MOSFETs for automotive ABS systems. In Proceedings of the 2008 IEEE Power Electronics Specialists Conference, Rhodes, Greece, 15–19 June 2008; pp. 1169–1175. [CrossRef]
99. Patil, S.; Waghmare, G. Determination of Thermal Induced Stresses in Semiconductor Chip Package by using Finite Element Analysis: A Brief Review. *Int. J. Eng. Res. Technol.* **2015**, *V4*, 44–47. [CrossRef]
100. Katsis, D.; vanWyk, J. A thermal, mechanical, and electrical study of voiding in the solder die-attach of power MOSFETs. *IEEE Trans. Components Packag. Technol.* **2005**, *29*, 127–136. [CrossRef]
101. Huang, H.; Mawby, P. A lifetime estimation technique for voltage source inverters. *IEEE Trans. Power Electron.* **2012**, *28*, 4113–4119. [CrossRef]
102. Nwanoro, K.; Lu, H.; Yin, C.; Bailey, C. An analysis of the reliability and design optimization of aluminium ribbon bonds in power electronics modules using computer simulation method. *Microelectron. Reliab.* **2018**, *87*, 1–14. [CrossRef]
103. Dusmez, S.; Akin, B. An accelerated thermal aging platform to monitor fault precursor on-state resistance. In Proceedings of the 2015 IEEE International Electric Machines & Drives Conference (IEMDC), Coeur d'Alene, ID, USA, 10–13 May 2015; pp. 1352–1358. [CrossRef]
104. Ciappa, M.; Fichtner, W. Lifetime prediction of IGBT modules for traction applications. In Proceedings of the 2000 IEEE International Reliability Physics Symposium Proceedings, 38th Annual (Cat. No. 00CH37059), San Jose, CA, USA, 10–13 April 2000; pp. 210–216. [CrossRef]
105. Ciappa, M. Selected failure mechanisms of modern power modules. *Microelectron. Reliab.* **2002**, *42*, 653–667. [CrossRef]
106. Cui, H. Accelerated temperature cycle test and Coffin-Manson model for electronic packaging. In Proceedings of the Annual Reliability and Maintainability Symposium, Alexandria, VA, USA, 24–27 January 2005; pp. 556–560. [CrossRef]
107. Bayerer, R.; Herrmann, T.; Licht, T.; Lutz, J.; Feller, M. Model for power cycling lifetime of IGBT modules—Various factors influencing lifetime. In Proceedings of the 5th International Conference on Integrated Power Electronics Systems, Nuremberg, Germany, 11–13 March 2008; pp. 37–42.
108. Scheuermann, U.; Schmidt, R. A new lifetime model for advanced power modules with sintered chips and optimized Al wire bonds. *PCIM Eur. Conf. Proc.* **2013**, *2013*, 810–817.
109. Wileman, A.; Perinpanayagam, S.; Aslam, S. Physics of failure (PoF) based lifetime prediction of power electronics at the printed circuit board level. *Appl. Sci.* **2021**, *11*, 2679. [CrossRef]
110. Ma, K.; Yang, Y.; Wang, H.; Blaabjerg, F. Design for reliability of power electronics in renewable energy systems. In *Use, Operation and Maintenance of Renewable Energy Systems*; Green Energy and Technology; Springer: Cham, Switzerland, 2014. [CrossRef]
111. Wang, H.; Ma, K.; Blaabjerg, F. Design for reliability of power electronic systems. In Proceedings of the IECON 2012—38th Annual Conference on IEEE Industrial Electronics Society, Montreal, QC, Canada, 25–28 October 2012; pp. 33–44. [CrossRef]
112. Ma, K.; Liserre, M.; Blaabjerg, F.; Kerekes, T. Thermal loading and lifetime estimation for power device considering mission profiles in wind power converter. *IEEE Trans. Power Electron.* **2014**, *30*, 590–602. [CrossRef]
113. Kovaltchouk, T.; Aubry, J.; Multon, B.; Ahmed, H. Influence of IGBT current rating on the thermal cycling lifetime of a power electronic active rectifier in a direct wave energy converter. In Proceedings of the 2013 15th European Conference on Power Electronics and Applications, Lille, France, 2–6 September 2013; pp. 1–10. [CrossRef]
114. Song, Y.; Wang, B. Evaluation Methodology and Control Strategies for Improving Reliability of HEV Power Electronic System. *IEEE Trans. Veh. Technol.* **2014**, *63*, 3661–3676. [CrossRef]
115. Murken, M.; Gratzfeld, P. Reliability Comparison of Bidirectional Automotive DC/DC Converters. In Proceedings of the 2017 IEEE 86th Vehicular Technology Conference (VTC-Fall), Toronto, ON, Canada, 24–27 September 2017; pp. 1–7. [CrossRef]
116. Ciappa, M.; Carbognani, F.; Cova, P.; Fichtner, W. A Novel Thermomechanics -Based Lifetime Prediction Model for Cycle Fatigue Failure Mechanisms in Power Semiconductors. *Microelectron. Reliab.* **2002**, *42*, 1653–1658. [CrossRef]
117. Mainka, K.; Thoben, M.; Schilling, O. Lifetime calculation for power modules, application and theory of models and counting methods. In Proceedings of the 2011 14th European Conference on Power Electronics and Applications, Birmingham, UK, 30 August 2011–1 September 2011; pp. 1–8.
118. Matsuichi, M.; Endo, T. Fatigue of metals subjected to varying stress. *Engineering* **1968**.
119. Lu, H.; Tilford, T.; Bailey, C.; Newcombe, D. Lifetime prediction for power electronics module substrate mount-down solder interconnect. In Proceedings of the International Symposium on High Density Packaging and Microsystem Integration, Shanghai, China, 26–28 June 2007. [CrossRef]
120. Miner, M.A. Cumulative Damage in Fatigue. *J. Appl. Mech.* **2021**, *12*, A159–A164. [CrossRef]
121. Schulz, M.; Xin, M. Correlating NTC-reading and chip-Temperature in power electronic modules. In Proceedings of the PCIM Europe 2015; International Exhibition and Conference for Power Electronics, Intelligent Motion, Renewable Energy and Energy Management, Nuremberg, Germany, 19–20 May 2015; pp. 19–21.
122. Motto, E.; Donlon, J. IGBT module with user accessible on-chip current and temperature sensors. In Proceedings of the 2012 Twenty-Seventh Annual IEEE Applied Power Electronics Conference and Exposition (APEC), Orlando, FL, USA, 5–9 February 2012; pp. 176–181. [CrossRef]

123. Wei, L.; McGuire, J.; Lukaszewski, R. Analysis of PWM frequency control to improve the lifetime of PWM inverter. *IEEE Trans. Ind. Appl.* **2010**, *47*, 922–929. [CrossRef]
124. Skibinski, G.; Sethares, W. Thermal Parameter Estimation Using Recursive Identification. *IEEE Trans. Power Electron.* **1991**, *6*, 228–239. [CrossRef]
125. Luo, Z.; Ahn, H.; ElNokali, M. A Thermal Model for Insulated Gate Bipolar Transistor Module. *IEEE Trans. Power Electron.* **2004**, *19*, 902–907. [CrossRef]
126. Prior, N. Wide Band-Gap Semiconductor Based Power Converter Reliability and Topology Investigation. In *Graduate Study in Criminology and Criminal Justice*, 1st ed.; Routledge: Abingdon, UK, 2020; pp. 212–213. [CrossRef]
127. *Transient Thermal Measurements and Thermal Equivalent Circuit Models*; AN 2015-10; Infineon: Neubiberg, Germany, 2015 ; pp. 1–13.
128. Brekel, W.; Duetemeyer, T.; Puk, G.; Schilling, O. Time resolved in situ Tvj measurements of 6.5 kV IGBTs during inverter operation. *Proc. PCIM Eur.* **2009**, 808–813.
129. Avenas, Y.; Dupont, L.; Khatir, Z. Temperature measurement of power semiconductor devices by thermo-sensitive electrical parameters—A review. *IEEE Trans. Power Electron.* **2011**, *27*, 3081–3092. [CrossRef]
130. Huai, W. Transitioning to physics-of-failure as a reliability driver in power electronics. *IEEE J. Emerg. Sel. Top. Power Electron.* **2013**, *2*, 97–114. [CrossRef]
131. Blackburn, D. Temperature measurements of semiconductor devices—A review. In Proceedings of the Annual IEEE Semiconductor Thermal Measurement and Management Symposium, San Jose, CA, USA, 11 March 2004; Volume 20, pp. 70–80. [CrossRef]
132. Stella, F.; Pellegrino, G.; Armando, E. Three-phase SiC inverter with active limitation of all MOSFETs junction temperature. *Microelectron. Reliab.* **2020**, *110*, 113659. [CrossRef]
133. Due, J.; Munk-Nielsen, S.; Nielsen, R. Lifetime investigation of high power IGBT modules. In Proceedings of the 2011 14th European Conference on Power Electronics and Applications, Birmingham, UK, 30 August 2011–1 September 2011.
134. Yang, F.; Ugur, E.; Akin, B. Evaluation of Aging's Effect on Temperature-Sensitive Electrical Parameters in SiC mosfets. *IEEE Trans. Power Electron.* **2019**, *35*, 6315–6331. [CrossRef]
135. Chen, H.; Pickert, V.; Atkinson, D.J.; Pritchard, L.S. On-line Monitoring of the MOSFET Device Junction Temperature by Computation of the Threshold Voltage. In Proceedings of the 3rd IET International Conference on Power Electronics, Machines and Drives (PEMD 2006), Dublin, Ireland, 4–6 April 2006; Volume 44, pp. 440–444.
136. Rasool, H.; Verbrugge, B.; Jaman, S.; Abramushkina, E.; Geury, T.; Baghdadi, M.E.; Hegazy, O. Design and Real-Time Implementation of a Control System for SiC Off-Board Chargers of Battery Electric Buses. *Energies* **2022**, *15*, 1–19. [CrossRef]
137. Xie, B.; Guo, K.; Mao, M.; Zhou, L.; Liu, T.; Zhang, Q.; Hao, G. Analysis and Improved Design of Phase Compensated Proportional Resonant Controllers for Grid-Connected Inverters in Weak Grid. *IEEE Trans. Energy Convers.* **2020**, *35*, 1453–1464. [CrossRef]
138. Ye, T.; Dai, N.Y.; Lam, C.S.; Wong, M.C.; Guerrero, J.M. Analysis, design, and implementation of a quasi-proportional-resonant controller for a multifunctional capacitive-coupling grid-connected inverter. *IEEE Trans. Ind. Appl.* **2016**, *52*, 4269–4280. [CrossRef]
139. Bayhan, S.; Komurcugil, H. Sliding-Mode Control Strategy for Three-Phase Three-Level T-Type Rectifiers with DC Capacitor Voltage Balancing. *IEEE Access* **2020**, *8*, 64555–64564. [CrossRef]
140. Kumar, M.; Huber, L.; Jovanović, M.M. Start-up procedure for three-phase six-switch boost PFC rectifier. In Proceedings of the 2014 IEEE Applied Power Electronics Conference and Exposition, Fort Worth, TX, USA, 16–20 March 2014; pp. 1852–1859. [CrossRef]
141. Mallik, A.; Lu, J.; Zou, S.; He, P.; Khaligh, A. Minimum inrush start-up control of a single-phase interleaved totem-pole PFC rectifier. In Proceedings of the 2018 IEEE Applied Power Electronics Conference and Exposition (APEC), San Antonio, TX, USA, 4–8 March 2018; pp. 754–759. [CrossRef]
142. Zhou, J.; Cheng, S.; Hu, Z.; Liu, J. Balancing control of neutral-point voltage for three-level T-type inverter based on hybrid variable virtual space vector. *IET Power Electron.* **2020**, *13*, 744–750. [CrossRef]
143. Song, Q.; Liu, W.H.; Yan, G.G.; Wang, Z.H. Neutral-point potential balancing algorithm for three-level NPC inverters by using analytically injected zero-sequence voltage. In Proceedings of the Eighteenth Annual IEEE Applied Power Electronics Conference and Exposition, Miami Beach, FL, USA, 9–13 February 2003; Volume 24, pp. 57–62. [CrossRef]
144. Jiao, Y.; Lee, F.C.; Lu, S. Space vector modulation for three-level NPC converter with neutral point voltage balance and switching loss reduction. *IEEE Trans. Power Electron.* **2014**, *29*, 5579–5591. [CrossRef]
145. Burgos, R.; Lai, R.; Pei, Y.; Wang, F.; Boroyevich, D.; Pou, J. Space Vector Modulation for Vienna-Type Rectifiers Based on the Equivalence between Two-and Three-Level Converters: A Carrier-Based Implementation. *IEEE Power Electron. Spec. Conf.* **2007**, *23*, 1888–1898. [CrossRef]
146. Zhang, M.; Yuan, Y.; Sun, X.; Zhang, Y.; Li, X. Harmonic Resonance Suppression Strategy of the Front-End Vienna Rectifier in EV Charging Piles. *IEEE Trans. Power Electron.* **2022**, *38*, 1036–1053. [CrossRef]
147. Rajendran, G.; Vaithilingam, C.A.; Misron, N.; Naidu, K.; Ahmed, M.R. Voltage oriented controller based vienna rectifier for electric vehicle charging stations. *IEEE Access* **2021**, *9*, 50798–50809. [CrossRef]
148. Nair, H.S.; Lakshminarasamma, N. An Improved FS-MPC Algorithm for Vienna Rectifier Based EV Chargers. In Proceedings of the 2020 IEEE Transportation Electrification Conference & Expo (ITEC), Chicago, IL, USA, 23–26 June 2020.
149. Qiu, X.; Li, Y.; Xu, H.; Lin, M.; Wu, S. *A Dual Closed-Loop Control Strategy Research Based on Sliding Mode Control for Vienna Rectifier*; Institute of Electrical and Electronics Engineers Inc.: Piscataway, NJ, USA, 2021; pp. 20–24. [CrossRef]

150. Kolar, J.W.; Friedli, T. The essence of three-phase PFC rectifier systemspart i. *IEEE Trans. Power Electron.* **2013**, *28*, 176–198. [CrossRef]
151. Soeiro, T.B.; Friedli, T.; Kolar, J.W. Design and implementation of a three-phase buck-type third harmonic current injection PFC rectifier SR. *IEEE Trans. Power Electron.* **2013**, *28*, 1608–1621. [CrossRef]
152. Zhang, B.; Xie, S.; Wang, X.; Xu, J. Modulation Method and Control Strategy for Full-Bridge-Based Swiss Rectifier to Achieve ZVS Operation and Suppress Low-Order Harmonics of Injected Current. *IEEE Trans. Power Electron.* **2020**, *35*, 6512–6522. [CrossRef]
153. Zhang, Q. An Improved Swiss Rectifier and Its Nonlinear Control for Lower THD. *CPSS Trans. Power Electron. Appl.* **2022**, *7*, 319–327. [CrossRef]
154. Jia, Q.; Qi, Y.; Xiong, X.; Ma, P. *Research and Implementation of SWISS Rectifier Based on Fuzzy PI Control*; Institute of Electrical and Electronics Engineers Inc.: Piscataway, NJ, USA, 2018; pp. 31–36. [CrossRef]
155. Chen, G.; Chen, Z.; Chen, Y.; Feng, C.; Zhu, X. Asymmetric Phase-Shift Modulation Strategy of DAB Converters for Improved Light-Load Efficiency. *IEEE Trans. Power Electron.* **2022**, *37*, 9104–9113. [CrossRef]
156. Vazquez, N.; Liserre, M. Peak Current Control and Feed-Forward Compensation for the DAB Converter. In Proceedings of the 2019 IEEE International Conference on Industrial Technology (ICIT): Melbourne Convention and Exhibition Centre, Melbourne, Australia, 13–15 February 2019; p. 1562.
157. Zou, S.; Mallik, A.; Lu, J.; Khaligh, A. Sliding Mode Control Scheme for a CLLC Resonant Converter. *IEEE Trans. Power Electron.* **2019**, *34*, 12274–12284. [CrossRef]
158. Zhu, T.; Zhuo, F.; Zhao, F.; Wang, F.; Yi, H.; Zhao, T. Optimization of Extended Phase-Shift Control for Full-Bridge CLLC Resonant Converter with Improved Light-Load Efficiency. *IEEE Trans. Power Electron.* **2020**, *35*, 11129–11142. [CrossRef]
159. Li, B.; Chen, M.; Wang, X.; Chen, N.; Sun, X.; Zhang, D. An Optimized Digital Synchronous Rectification Scheme Based on Time-Domain Model of Resonant CLLC Circuit. *IEEE Trans. Power Electron.* **2021**, *36*, 10933–10948. [CrossRef]
160. Li, Z.; Wu, T.; Zhang, G.; Yang, R. Hybrid modulation method combining variable frequency and double phase-shift for a 10 kW LLC resonant converter. *IET Power Electron.* **2018**, *11*, 2161–2169. [CrossRef]
161. Gui, H.D.; Zhang, Z.; He, X.F.; Liu, Y.F. *A High Voltage-Gain LLC Micro-Converter with High Efficiency in Wide Input Range for PV Applications*; Institute of Electrical and Electronics Engineers Inc.: Piscataway, NJ, USA, 2014; pp. 637–642. [CrossRef]
162. Wei, Y.; Luo, Q.; Mantooth, A. Comprehensive Analysis and Design of LLC Resonant Converter With Magnetic Control. *CPSS Trans. Power Electron. Appl.* **2019**, *4*, 265–275. [CrossRef]
163. Alonso, J.M.; Perdigão, M.S.; Vaquero, D.G.; Calleja, A.J.; Saraiva, E.S. Analysis, design, and experimentation on constant-frequency DC-DC resonant converters with magnetic control. *IEEE Trans. Power Electron.* **2012**, *27*, 1369–1382. [CrossRef]
164. Wu, H.; Mu, T.; Gao, X.; Xing, Y. A secondary-side phase-shift-controlled LLC resonant converter with reduced conduction loss at normal operation for hold-up time compensation application. *IEEE Trans. Power Electron.* **2015**, *30*, 5352–5357. [CrossRef]
165. Zong, S.; Luo, H.; Li, W.; Deng, Y.; He, X. Asymmetrical Duty Cycle-Controlled LLC Resonant Converter with Equivalent Switching Frequency Doubler. *IEEE Trans. Power Electron.* **2016**, *31*, 4963–4973. [CrossRef]
166. Park, H.P.; Jung, J.H. PWM and PFM Hybrid Control Method for LLC Resonant Converters in High Switching Frequency Operation. *IEEE Trans. Ind. Electron.* **2017**, *64*, 253–263. [CrossRef]
167. Murdock, D.; Torres, J.; Connors, J.; Lorenz, R. Active thermal control of power electronic modules. *IEEE Trans. Ind. Appl.* **2005**, *42*, 552–558. [CrossRef]
168. Lemmens, J.; Driesen, J.; Vanassche, P. Thermal management in traction applications as a constraint optimal control problem. In Proceedings of the 2012 IEEE Vehicle Power and Propulsion Conference, VPPC 2012, Seoul, Republic of Korea, 12 October 2012; pp. 36–41. [CrossRef]
169. Yang, Y.; Koutroulis, E.; Sangwongwanich, A.; Blaabjerg, F. Minimizing the levelized cost of energy in single-phase photovoltaic systems with an absolute active power control. In Proceedings of the 2015 IEEE Energy Conversion Congress and Exposition, Montreal, QC, Canada, 20–24 September 2015; pp. 28–34. [CrossRef]
170. Castellazzi, A.; Onifade, M.; Wang, X.; Zanchetta, P. State-space modeling of power assemblies for advanced thermal management solutions. In Proceedings of the 2012 IEEE 13th Workshop on Control and Modeling for Power Electronics, COMPEL 2012, Kyoto, Japan, 10 July 2012. [CrossRef]
171. Wang, X.; Castellazzi, A.; Zanchetta, P. Regulated cooling for reduced thermal cycling of power devices. In Proceedings of the 2012 IEEE 7th International Power Electronics and Motion Control Conference—ECCE, Novi Sad, Serbia, 4–6 September 2012; Volume 1, pp. 238–244. [CrossRef]
172. Davidson, J.N.; Stone, D.A.; Foster, M.P. Real-time temperature monitoring and control for power electronic systems under variable active cooling by characterisation of device thermal transfer impedance. In Proceedings of the 7th IET International Conference on Power Electronics, Machines and Drives (PEMD 2014), Manchester, UK, 8–10 April 2014. [CrossRef]
173. Falck, J.; Andresen, M.; Liserre, M. Active thermal control of IGBT power electronic converters. In Proceedings of the IECON 2015—41st Annual Conference of the IEEE Industrial Electronics Society, Yokohama, Japan, 28 January 2016; Volume 1, pp. 1–6. [CrossRef]
174. Andresen, M.; Buticchi, G.; Falck, J.; Liserre, M.; Muehlfeld, O. Active thermal management for a single-phase H-Bridge inverter employing switching frequency control. In Proceedings of the PCIM Europe 2015, International Exhibition and Conference for Power Electronics, Intelligent Motion, Renewable Energy and Energy Management, Nuremberg, Germany, 19–20 May 2015; pp. 1–8.

175. Vernica, I.; Blaabjerg, F.; Ma, K. Modelling and design of active thermal controls for power electronics of motor drive applications. In Proceedings of the IEEE Applied Power Electronics Conference and Exposition—APEC, New Orleans, LO, USA, 15–19 March 2020; pp. 2902–2909. [CrossRef]
176. Wu, J.; Zhou, L.; Sun, P.; Du, X. Smooth control of insulated gate bipolar transistors junction temperature in a small-scale wind power converter. *IET Power Electron.* **2014**, *9*, 393–400. [CrossRef]
177. Prasobhu, P.; Raveendran, V.; Buticchi, G.; Liserre, M. Active Thermal Control of GaN-Based DC/DC Converter. *IEEE Trans. Ind. Appl.* **2018**, *54*, 3529–3540. [CrossRef]
178. Blasko, V.; Lukaszewski, R.; Sladky, R. On line thermal model and thermal management strategy of a three phase voltage source inverter. In Proceedings of the Conference Record—IAS Annual Meeting (IEEE Industry Applications Society), Las Vegas, NV, USA, 7–11 October 2012; Volume 2, pp. 1423–1431. [CrossRef]
179. Lemmens, J.; Vanassche, P.; Driesen, J. Optimal Control of Traction Motor Drives Under Electrothermal Constraints. *IEEE J. Emerg. Sel. Top Power Electron.* **2014**, *2*, 249–263. [CrossRef]
180. Calzo, G.; Lidozzi, A.; Solero, L.; Crescimbini, F.; Cardi, V. Thermal regulation as control reference in electric drives. In Proceedings of the 15th International Power Electronics and Motion Control Conference and Exposition, EPE-PEMC 2012 ECCE Europe, Novi Sad, Serbia, 4–6 September 2012; pp. 1–7. [CrossRef]
181. Weckert, M.; Roth-Stielow, J. Lifetime as a control variable in power electronic systems. In Proceedings of the 2010 Emobility—Electrical Power Train EEPT, Leipzig, Germany, 13 December 2010; pp. 8–13. [CrossRef]
182. Ma, K.; Liserre, M.; Blaabjerg, F. Reactive Power Influence on the Thermal Cycling of Multi-MW Wind Power Inverter. *IEEE Trans. Ind. Appl.* **2013**, *49*, 922–930. [CrossRef]
183. Dusmez, S.; Akin, B. An Active Life Extension Strategy for Thermally Aged Power Switches Based on the Pulse-Width Adjustment Method in Interleaved Converters. *IEEE Trans. Power Electron.* **2015**, *31*, 5149–5160. [CrossRef]
184. Ma, K.; Blaabjerg, F. Modulation methods for neutral-point-clamped wind power converter achieving loss and thermal redistribution under low-voltage ride-through. *IEEE Trans. Ind. Electron.* **2013**, *61*, 835–845. [CrossRef]
185. Ma, K.; Blaabjerg, F. Thermal optimised modulation methods of three-level neutral-point-clamped inverter for 10 MW wind turbines under low-voltage ride through. *IET Power Electron.* **2011**, *5*, 920–927. [CrossRef]
186. Phan, T.; Oikonomou, N.; Riedel, G.; Pacas, M. PWM for active thermal protection in three level neutral point clamped inverters. In Proceedings of the IEEE Energy Conversion Congress and Exposition, ECCE, Detroit, MI, USA, 9 October 2022; pp. 3710–3716. [CrossRef]
187. Aly, M.; Ahmed, E.; Shoyama, M. Thermal stresses relief carrier-based PWM strategy for single-phase multilevel inverters. *IEEE Trans. Power Electron.* **2017**, *32*, 9376–9388. [CrossRef]
188. Ko, Y.; Andresen, M.; Buticchi, G.; Liserre, M. Thermally Compensated Discontinuous Modulation Strategy for Cascaded H-Bridge Converters. *IEEE Trans. Power Electron.* **2017**, *33*, 2704–2713. [CrossRef]
189. Ko, Y.; Andresen, M.; Buticchi, G.; Lee, J.; Liserre, M. Modulation strategy for highly reliable cascade H-Bridge inverter based on discontinuous PWM. In Proceedings of the Conference Proceedings—IEEE Applied Power Electronics Conference and Exposition—APEC, Houston, TX, USA, 19 May 2022; pp. 3241–3246. [CrossRef]
190. Dusmez, S.; Ugur, E.; Akin, B. Power switch lifetime extension strategies for three-phase converters. In Proceedings of the Conference Proceedings—IEEE Applied Power Electronics Conference and Exposition—APEC, Houston, TX, USA, 19 May 2022; pp. 1176–1182. [CrossRef]
191. Wu, L.; Castellazzi, A. Temperature adaptive driving of power semiconductor devices. In Proceedings of the IEEE International Symposium on Industrial Electronics, Anchorage, AK, USA, 25 July 2022; pp. 1110–1114. [CrossRef]
192. Ruthardt, J.; Fischer, M.; Felix Woelfle, J.; Troester, N.; Roth-Stielow, J. Three-Level-Gate-Driver to Run Power Transistors in the Saturation Region for Junction Temperature Control. In Proceedings of the PCIM Europe 2018; International Exhibition and Conference for Power Electronics, Intelligent Motion, Renewable Energy and Energy Management, Nuremberg, Germany, 5–7 June 2018; pp. 1–8.
193. Wang, L.; Vermulst, B.; Duarte, J.; Huisman, H. Thermal stress reduction of power MOSFET in electric drive application with dynamic gate driving strategy. In Proceedings of the IEEE Applied Power Electronics Conference and Exposition—APEC, Houston, TX, USA, 19 May 2022; pp. 720–727. [CrossRef]
194. Wang, L.; Vermulst, B.; Duarte, J. Multilevel Gate Driver with Adjustable Gate Voltage for Thermal Stress Reduction of Power Switches in Electric Drive Application. In Proceedings of the International Exhibition and Conference for Power Electronics, Intelligent Motion, Renewable Energy and Energy Management, Nuremburg, Germany, 7–8 July 2020; pp. 1–8.
195. Wang, L.; Vermulst, B.; Duarte, J.; Huisman, H. Thermal stress reduction of power mosfet with dynamic gate voltage control and circulation current injection in electric drive application. *Electronics* **2020**, *9*, 1–22. [CrossRef]
196. Wang, L.; Vermulst, B.; Duarte, J.; Huisman, H. Thermal stress reduction and lifetime improvement of power switches with dynamic gate driving strategy. In Proceedings of the 21st European Conference on Power Electronics and Applications, EPE 2019 ECCE Europe, Genova, Italy, 28 November 2019. [CrossRef]
197. Ruthardt, J.; Hermann, C.; Wölfle, J.; Fischer, M.; Roth-Stielow, J. Gate-driver circuit with a variable supply voltage to influence the switching losses. *J. Eng.* **2018**, *2019*, 3692–3695. [CrossRef]

198. Luo, H.; Iannuzzo, F.; Ma, K.; Blaabjerg, F.; Li, W.; He, X. Active gate driving method for reliability improvement of IGBTs via junction temperature swing reduction. In Proceedings of the 2016 IEEE 7th International Symposium on Power Electronics for Distributed Generation Systems, PEDG 2016, Vancouver, BC, Canada, 27–30 June 2016. [CrossRef]
199. Broeck, C.; Ruppert, L.; Lorenz, R.; Doncker, R. Active thermal cycle reduction of power modules via gate resistance manipulation. In Proceedings of the Conference Proceedings—IEEE Applied Power Electronics Conference and Exposition—APEC, Houston, TX, USA, 20–24 March 2022; pp. 3074–3082. [CrossRef]
200. Sintamarean, N.C. *Reliability Oriented Circuit Design For Power Electronics Applications*; Aalborg University: Aalborg Øst, Denmark, 2015.
201. Baker, N.; Munk-Nielsen, S.; Liserre, M.; Iannuzzo, F. Online junction temperature measurement via internal gate resistance during turn-on. In Proceedings of the 2014 16th European Conference on Power Electronics and Applications, Lappeenranta, Finland, 26–28 August 2014; pp. 1–10. [CrossRef]
202. Baker, N.; Dupont, L.; Munk-Nielsen, S.; Iannuzzo, F.; Liserre, M. IR camera validation of IGBT junction temperature measurement via peak gate current. *IEEE Trans. Power Electron.* **2016**, *32*, 3099–3111. [CrossRef]
203. Baker, N.; Munk-Nielsen, S.; Iannuzzo, F.; Liserre, M. IGBT Junction Temperature Measurement via Peak Gate Current. *IEEE Trans. Power Electron.* **2015**, *31*, 3784–3793. [CrossRef]
204. Chen, H.; Ji, B.; Pickert, V.; Cao, W. Real-time temperature estimation for power MOSFETs considering thermal aging effects. *IEEE Trans. Device Mater. Reliab.* **2013**, *14*, 220–228. [CrossRef]
205. Bahun, I.; Sunde, V.; Jacapovic, Z. Estimation of insulated-gate bipolar transistor operating temperature: Simulation and experiment. *J. Power Electron.* **2013**, *13*, 729–736. [CrossRef]
206. Strauss, B.; Lindemann, A. Measuring the junction temperature of an IGBT using its threshold voltage as a temperature sensitive electrical parameter (TSEP). In Proceedings of the 2016 13th International Multi-Conference on Systems, Signals & Devices, Leipzig, Germany, 21–24 March 2016; pp. 459–467. [CrossRef]
207. Bahun, I.; Cobanov, N.; Jakopovic, Z. Real-time measurement of IGBT's operating temperature. *Automatika* **2011**, *52*, 295–305. [CrossRef]
208. Zhang, Z.; Wang, F.; Costinett, D.; Tolbert, L.; Blalock, B.; Wu, X. Online junction temperature monitoring using turn-off delay time for silicon carbide power devices. In Proceedings of the ECCE 2016—IEEE Energy Conversion Congress and Exposition, Milwaukee, WI, USA, 8–22 September 2016. [CrossRef]
209. Kuhn, H.; Mertens, A. On-line junction temperature measurement of IGBTs based on temperature sensitive electrical parameters. In Proceedings of the 13th European Conference on Power Electronics and Applications, Barcelona, Spain, 8–10 September 2009.
210. Sundaramoorthy, V.; Bianda, E.; Bloch, R.; Nistor, I.; Knapp, G.; Heinemann, A. Online estimation of IGBT junction temperature (Tj) using gate-emitter voltage (Vge) at turn-off. In Proceedings of the 15th European Conference on Power Electronics and Applications, Geneva, Switzerland, 8–10 September 2015. [CrossRef]
211. Sun, P. Online junction temperature extraction with turn-off delay time for high power IGBTs. In Proceedings of the 2014 IEEE Energy Conversion Congress and Exposition, ECCE 2014, Pittsburgh, PA, USA, 14–18 September 2014; pp. 4016–4021. [CrossRef]
212. Barlini, D.; Ciappa, M.; Mermet-Guyennet, M.; Fichtner, W. Measurement of the transient junction temperature in MOSFET devices under operating conditions. *Microelectron. Reliab.* **2007**, *47*, 1707–1712. [CrossRef]
213. Luo, H.; Chen, Y.; Sun, P.; Li, W.; He, X. Junction Temperature Extraction Approach with Turn-off Delay Time for High-voltage High-Power IGBT Modules. *IEEE Trans. Power Electron.* **2015**, *31*, 5122–5132. [CrossRef]
214. Yang, F.; Pu, S.; Xu, C.; Akin, B. A System Level Approach for Online Junction Temperature Measurement of SiC MOSFETs Using Turn-On Delay Time. In Proceedings of the 2020 IEEE Transportation Electrification Conference and Expo, Chicago, IL, USA, 21–25 June 2021; pp. 1012–1017. [CrossRef]
215. Barlini, D.; Ciappa, M.; Castellazzi, A.; Mermet-Guyennet, M.; Fichtner, W. New technique for the measurement of the static and of the transient junction temperature in IGBT devices under operating conditions. *Microelectron. Reliab.* **2006**, *46*, 1772–1777. [CrossRef]
216. Niu, H.; Lorenz, R. Real-Time Junction Temperature Sensing for Silicon Carbide MOSFET with Different Gate Drive Topologies and Different Operating Conditions. *IEEE Trans. Power Electron.* **2017**, *33*, 3424–3440. [CrossRef]
217. Koenig, A.; Plum, T.; Fidler, P.; De Doncker, R.W. On-line Junction Temperature Measurement of CoolMOS Devices. In Proceedings of the 2007 7th International Conference on Power Electronics and Drive Systems, Bangkok, Thailand, 27–30 November 2007; pp. 90–95. [CrossRef]
218. Zhang, Y.; Liang, Y. A simple approach on junction temperature estimation for SiC MOSFET dynamic operation within safe operating area. In Proceedings of the 2015 IEEE Energy Conversion Congress and Exposition (ECCE), Montreal, QC, Canada, 20–24 September 2015; pp. 5704–5707. [CrossRef]
219. Hosseinabadi, F. Implementation of onsite Junction Temperature Estimation for a SiC MOSFET Module for Condition Monitoring. In Proceedings of the 2022 24th European Conference on Power Electronics and Applications (EPE'22 ECCE Europe), Hanover, Germany, 5–9 September 2022; pp. 1– 6.
220. Gonzalez, J.; Alatise, O.; Hu, J.; Ran, L.; Mawby, P. Temperature sensitive electrical parameters for condition monitoring in SiC power MOSFETs. *IET Conf. Publ.* **2016**, *2016*, 1–6. [CrossRef]
221. Ma, D.; Chen, W.; Ruan, X. A Review of Voltage/Current Sharing Techniques for Series-Parallel-Connected Modular Power Conversion Systems. *IEEE Trans. Power Electron.* **2020**, *35*, 12383–12400. [CrossRef]

222. Kolar, J.W.; Krismer, F.; Lobsiger, Y.; Muhlethaler, J.; Nussbaumer, T.; Minibock, J. Extreme efficiency power electronics. In Proceedings of the 2012 7th International Conference on Integrated Power Electronics Systems (CIPS), Nuremberg, Germany, 6–8 March 2012; pp. 1–22.
223. Karlsson, P.; Svensson, J. DC Bus Voltage Control for a Distributed Power System. *IEEE Trans. Power Electron.* **2003**, *18*, 1405–1412. [CrossRef]
224. Peyghami, S.; Davari, P.; Blaabjerg, F. System-level lifetime-oriented power sharing control of paralleled DC/DC converters. In Proceedings of the Conference Proceedings—IEEE Applied Power Electronics Conference and Exposition—APEC, Orlando, FL, USA, 19–23 March 2023; pp. 1890–1895. [CrossRef]
225. Peyghami, S.; Blaabjerg, F. *Reliability/Cost-Based Power Routing in Power Electronic-based Power Systems*; Institute of Electrical and Electronics Engineers Inc.: Piscataway, NJ, USA, 2021; pp. 789–795. [CrossRef]
226. Raveendran, V.; Andresen, M.; Liserre, M. Improving onboard converter reliability for more electric aircraft with lifetime-based control. *IEEE Trans. Ind. Electron.* **2019**, *66*, 5787–5796. [CrossRef]
227. Liu, X.; Zhang, Y.; Cao, R.; Li, Y.; Lv, C.; Liu, J. *Capacitor Damage-Based Power Routing Strategy in ISOP-DAB Converters for Smart Grid*; Institute of Electrical and Electronics Engineers Inc.: Piscataway, NJ, USA, 2021; pp. 1783–1788. [CrossRef]
228. Stroe, D.I.; Swierczynski, M.; Stan, A.I.; Teodorescu, R.; Andreasen, S.J. Accelerated lifetime testing methodology for lifetime estimation of lithium-ion batteries used in augmented wind power plants. *IEEE Trans. Ind. Appl.* **2014**, *50*, 4006–4017. [CrossRef]
229. Chu, A.; Allam, A.; Arenas, A.C.; Rizzoni, G.; Onori, S. Stochastic capacity loss and remaining useful life models for lithium-ion batteries in plug-in hybrid electric vehicles. *J. Power Sources* **2020**, *478*, 228991. [CrossRef]
230. Li, J.; Xiong, R.; Mu, H.; Cornélusse, B.; Vanderbemden, P.; Ernst, D.; Yuan, W. Design and real-time test of a hybrid energy storage system in the microgrid with the benefit of improving the battery lifetime. *Appl. Energy* **2018**, *218*, 470–478. [CrossRef]
231. Zhang, J.; Zhang, L.; Sun, F.; Wang, Z. An Overview on Thermal Safety Issues of Lithium-ion Batteries for Electric Vehicle Application. *IEEE Access* **2018**, *6*, 23848–23863. [CrossRef]
232. TIDA-01606. 10-kW, Bidirectional Three-Phase Three-Level (T-type) Inverter and PFC Reference Design, 2021. Available online: https://www.ti.com/lit/ug/tidue53h/tidue53h.pdf?ts=1675664546647&ref_url=https%253A%252F%252Fwww.google.com%252F (accessed on 17 November 2022).
233. Chen, B.; Liang, X.; Wan, N. Design Methodology for Inductor-Integrated Litz-Wired High-Power Medium-Frequency Transformer with the Nanocrystalline Core Material for Isolated DC-Link Stage of Solid-State Transformer. *IEEE Trans. Power Electron.* **2020**, *35*, 11557–11573. [CrossRef]
234. Stojadinovic, M.; Biela, J. *Modelling and Design of a Medium Frequency Transformer for High Power DC-DC Converters*; Institute of Electrical and Electronics Engineers Inc.: Piscataway, NJ, USA, 2018; pp. 1103–1110. [CrossRef]
235. Abramushkina, E.; Zhaksylyk, A.; Geury, T.; Baghdadi, M.E.; Hegazy, O. A thorough review of cooling concepts and thermal management techniques for automotive wbg inverters: Topology, technology and integration level. *Energies* **2021**, *14*, 4981. [CrossRef]
236. Zhao, G.; Wang, X.; Negnevitsky, M.; Zhang, H. A review of air-cooling battery thermal management systems for electric and hybrid electric vehicles. *J. Power Sources* **2021**, *501*, 230001. [CrossRef]
237. Wang, X.; Liu, S.; Zhang, Y.; Lv, S.; Ni, H.; Deng, Y.; Yuan, Y. A Review of the Power Battery Thermal Management System with Different Cooling, Heating and Coupling System. *Energies* **2022**, *15*, 1963. [CrossRef]
238. Wu, W.; Wang, S.; Wu, W.; Chen, K.; Hong, S.; Lai, Y. A critical review of battery thermal performance and liquid based battery thermal management. *Energy Convers. Manag.* **2019**, *182*, 262–281. [CrossRef]
239. Wazeer, A.; Das, A.; Abeykoon, C.; Sinha, A.; Karmakar, A. Phase change materials for battery thermal management of electric and hybrid vehicles: A review. *Energy Nexus* **2022**, *7*, 100131. [CrossRef]
240. Lamprecht, A.; Garikapati, A.; Narayanaswamy, S.; Machleid, J.; Steinhorst, S. On the efficacy of SoC-preconditioning on the utilization of battery packs in Electric Vehicles. *Microprocess. Microsyst.* **2022**, *88*, 103711. [CrossRef]
241. Bui, T.M.; Sheikh, M.; Dinh, T.Q.; Gupta, A.; Widanalage, D.W.; Marco, J. A Study of Reduced Battery Degradation through State-of-Charge Pre-Conditioning for Vehicle-to-Grid Operations. *IEEE Access* **2021**, *9*, 155871–155896. [CrossRef]
242. Lin, X.; Khosravinia, K.; Hu, X.; Li, J.; Lu, W. Lithium Plating Mechanism, Detection, and Mitigation in Lithium-Ion Batteries. *Prog. Energy Combust. Sci.* **2021**, *87*, 100953. [CrossRef]
243. Chen, S.; Bao, N.; Garg, A.; Peng, X.; Gao, L. A Fast Charging–Cooling Coupled Scheduling Method for a Liquid Cooling-Based Thermal Management System for Lithium-Ion Batteries. *Engineering* **2021**, *7*, 1165–1176. [CrossRef]
244. Kleiner, J.; Stuckenberger, M.; Komsiyska, L.; Endisch, C. Advanced monitoring and prediction of the thermal state of intelligent battery cells in electric vehicles by physics-based and data-driven modeling. *Batteries* **2021**, *7*, 31. [CrossRef]
245. Lee, C.H.; Wu, Z.Y.; Hsu, S.H.; Jiang, J.A. Cycle Life Study of Li-Ion Batteries with an Aging-Level-Based Charging Method. *IEEE Trans. Energy Convers.* **2020**, *35*, 1475–1484. [CrossRef]
246. Gao, Z.; Xie, H.; Yang, X.; Niu, W.; Li, S.; Chen, S. The Dilemma of C-Rate and Cycle Life for Lithium-Ion Batteries under Low Temperature Fast Charging. *Batteries* **2022**, *8*, 234. [CrossRef]